Glutamatergic Supramammillary Nucleus Neurons Respond to Threatening Stressors and Promote Active Coping

Abraham Escobedo[1], Salli-Ann Holloway[1], Megan Votoupal[2], Aaron L Cone[1], Hannah E Skelton[1], Alex A. Legaria[3,4], Imeh Ndiokho[5], Tasheia Floyd[6], Alexxai V. Kravitz[1,3,4], Michael R. Bruchas[7,8,9,10, *], Aaron J. Norris[1*]

Affiliations:

1 Department of Anesthesiology, Washington University in St. Louis, St. Louis, MO

2 Department of Medicine, Northwestern University Feinberg School of Medicine, Chicago IL

3 Department of Neuroscience, Washington University in St. Louis, St. Louis, MO

4 Department of Psychiatry, Washington University in St. Louis, St. Louis, MO

5 Medical College of Wisconsin, Milwaukee WI

6 Department of Obstetrics and Gynecology, Washington University in St. Louis, St. Louis, MO

7 Center for Neurobiology of Addiction, Pain, and Emotion University of Washington, Seattle, WA

8 Department of Anesthesiology and Pain Medicine University of Washington, Seattle, WA

9 Department of Pharmacology University of Washington, Seattle, WA

10 Department of Bioengineering University of Washington, Seattle, WA

* Corresponding authors

Lead Contact:

Aaron Norris

660 S. Euclid Ave

Saint Louis, MO 63110

norris@wustl.edu

(314) 273-4422

Abstract:

Threat-response neural circuits are conserved across species and play roles in normal behavior and psychiatric diseases. Maladaptive changes in these neural circuits contribute to stress, mood, and anxiety disorders. Active coping in response to stressors is a psychosocial factor associated with resilience against stress-induced mood and anxiety disorders. The neural circuitry underlying active coping is poorly understood, but the functioning of these circuits could be key for overcoming anxiety and related disorders. The supramammillary nucleus (SuM) has been suggested to be engaged by threat. SuM has many projections and contains a poorly understood diversity of populations. We identified a unique population of glutamatergic SuM neurons ($SuM^{VGLUT2+}$::POA) based on projection to the preoptic area of the hypothalamus (POA) and found $SuM^{VGLUT2+}$::POA neurons have extensive arborizations. $SuM^{VGLUT2+}$::POA neurons project to brain areas that mediate various features of the stress and threat responses including the paraventricular nucleus thalamus (PVT), periaqueductal gray (PAG), and the habenula (Hb). Thus, $SuM^{VGLUT2+}$::POA neurons are positioned as a hub, connecting to areas implicated in regulating stress responses. Here we report $SuM^{VGLUT2+}$::POA neurons are recruited by diverse threatening stressors, and recruitment of $SuM^{VGLUT2+}$::POA neurons correlated with active coping behaviors. We found that selective photoactivation of the $SuM^{VGLUT2+}$::POA population drove aversion but not anxiety like behaviors. Activation of $SuM^{VGLUT2+}$::POA neurons in the absence of acute stressors evoked active coping like behaviors and drove instrumental behavior (selective port activations) (**Figure 6**). Also, activation of $SuM^{VGLUT2+}$::POA neurons was sufficient to convert passive coping strategies to active behaviors during acute stress. In contrast, we found activation of GABAergic (VGAT+) SuM neurons (SuM^{VGAT+}) neurons did not alter drive aversion or active coping, but termination of photostimulation was followed by increased mobility in the forced swim test. These findings establish a new node in stress response circuitry that has projections to many brain areas, evokes flexible active coping behaviors, and offers new opportunities for furthering our neurobiological understanding of stress.

Introduction

Threat-response neural circuits are conserved across species and have roles in normal behaviors and psychiatric diseases[1-4]. Identifying and responding to threatening stressors is critical for survival, but maladaptive changes in underlying neural circuits can contribute to stress, mood, and anxiety disorders[5, 6]. Active coping in response to stressors is a psychosocial factor associated with resilience against stress induced mood and anxiety disorders [7]. Available evidence indicates that active (e.g., escape, fighting) and passive (e.g., freezing, immobility) coping responses to stressors are governed by separable neural circuits[1, 8, 9]. The functioning of circuits underlying active coping could be key for overcoming anxiety and related disorders[10, 11].The neural circuits, cells, and mechanisms underlying active coping strategies remain unclear[12, 13].

The supramammillary nucleus (SuM) has been suggested to be engaged by threatening stressors and has efferent connections to stress-sensitive brain regions so may be an important regulator of responses to stressors[14-16]. Research on SuM has focused on connections to the hippocampus and septum while SuM projections to other brain areas remain less understood[15, 17, 18]. SuM contains distinct populations with functionally diverse roles including regulation of hippocampal activity during REM, spatial memory, arousal, and environmental interactions[19-23]. In addition to functional diversity, anatomical and molecular-cellular diversity is present in SuM[24-26]. Divergent populations in SuM have been defined by differential to the dentate gyrus and CA2 regions of the hippocampus, and neurochemically based on neurotransmitter expression[27, 28]. Major projections from the SuM, which have yet to be examined, include the preoptic hypothalamus area (POA). We examined if SuM neurons projected to the POA and if this projection could be used to aid in separation of populations in SuM.

We used retrograde adeno associated viral (AAV) and combinatorial genetic tools to identify and characterize a population of glutamatergic SuM neurons with projections to the POA ($SuM^{VGLUT2+}$::POA). We found that $SuM^{VGLUT2+}$::POA neurons represented an anatomical subset of SuM neurons with extensive arborizations to brain regions including those that mediate stress and threat responses including the paraventricular nucleus (PVT), periaqueductal gray (PAG), and the habenula (Hb). Thus, $SuM^{VGLUT2+}$::POA neurons are positioned as hubs with spokes to many areas regulating responses to threatening stressors. We hypothesized this population could respond to and regulate responses to stressors. We found $SuM^{VGLUT2+}$::POA neurons are recruited by multiple types of acute threatening stressors, encode a negative valance, do not promote anxiety-like behaviors, and evoke active coping behaviors. Further, activation of these $SuM^{VGLUT2+}$::POA neurons was sufficient to convert passive coping strategies to active behaviors.

These findings indicate SuM$^{VGLUT2+}$::POA neurons are a central hub linked to multiple stress and threat responsive areas and can drive state transitions between passive and active responses to stress.

Results

VGLUT2+ SuM neurons projecting to the POA (SuM$^{VGLUT2+}$::POA) arborize to multiple stress-engaged brain regions

The SuM contains functionally diverse and anatomically distinct populations with efferent projections to many brain regions[16, 24, 29, 30]. The diversity includes glutamatergic, GABAergic, and co-expressing GABAergic/Glutamatergic populations[21, 31]. Using retrograde adeno associated virus (Retro-AAV) (Retro-AAV2-DIO-tdTomato) and anterograde (AAV5-DIO-ChR2eYFP) tracing we identified a population of VGLUT2+ expressing neurons in SuM that project to the POA (SuM$^{VGLUT2+}$::POA) with dense projections in the lateral preoptic area (LPO) within the POA (**Supplemental Figure 1A-F**) in VGLUT2-Cre mice (n=4). Using a viral construct encoding for a nuclear restricted fluorophore that switches from mCherry (red) to eGFP (green) in a Cre-dependent manner (Retro-AAV2-Nuc-flox(mCherry)-eGFP), we found SuM$^{VGLUT2+}$::POA neurons were positive for VGLUT2+ in VGLUT2-Cre mice (n=4) and negative for VGAT expression in VGAT-Cre mice (n=3) (**Supplemental Figure 1G-L**) indicating that SuM$^{\mathbf{VGLUT2}}$::POA neurons do not belong to a GABAergic/Glutamatergic populations.

To examine arborization of SuM$^{VGLUT2+}$::POA neurons we utilized a combinatorial genetic approach. Specifically, we used mice (VGLUT2-Flp) that express Flp recombinase in VGLUT2 expressing cells in a combination with Flp dependent expression (fDIO) of Cre and Cre (DIO) dependent fluorophore expression. We injected Retro-AAV2-DIO-eYFP into POA and AAV-fDIO-Cre in to SuM (**Figure 1A**). We thus expressed Cre in SuM$^{VGLUT2+}$ neurons and, of those, only neurons projecting to the POA (SuM^{VGLUT2}::POA neurons) were labeled with eYFP. We found SuM^{VGLUT2}::POA neurons arborize widely, projecting to multiple brain regions including: the nucleus accumbens (Acb), Septum, lateral hypothalamus (LH), ventral medial hypothalamus (VMH), paraventricular nucleus (PVT), lateral habenula (lHb), the ventral lateral periaqueductal gray (VLPAG), dorsal raphe (DRD), lateral parabrachial nucleus (LPBN), laterodorsal tegmental nucleus (LDTg), and medial vestibular nucleus (MVe) (**Figure 1 D-M**). We visualized arborization of SuM^{VGLUT2}::POA neurons in cleared tissue by using optical light sheet imaging. For these experiments we injected VGLUT2-Flp mice (n=3) as in Figure 1A and brains were actively cleared using SHIELD for optical light sheet imaging[32]. Compiled three-dimensional images of a brain hemisphere, viewed from the medial to lateral perspective (**Figure 1M**) or viewed from the ventral

93 to dorsal perspective (**Supplemental Figure 2M**), showed projections labeled by eYFP from
94 SuM$^{VGLUT2+}$::POA to POA, areas of hippocampus, septum, Acb, and regions in the pons and
95 midbrain. The results further established projections from SuM$^{VGLUT2+}$::POA neurons to multiple
96 brain areas and illustrate the broad arborization.

97 We used tracing with Retro-AAV's to further corroborate our findings from anterograde
98 tracing by injecting unilaterally into the Acb, septum, PVT, or PAG in VGLUT2-Cre mice. Cell
99 bodies in SuM were labeled eYFP or tdTomato (**Supplemental Figure 2A-L**). Each area was
100 injected in three or more mice, yielding similar results. We examined the anatomic distribution of
101 SuM::POA neurons in SuM by injecting Retro-AAV2-Cre into the POA and AAV5-Nuc-
102 flox(mCherry)-eGFP into the SuM (**Supplemental Figure 3 A-B**) of wildtype (WT) Cre- mice (n=3)
103 In mice injected with this combination of viruses, we observed neurons labeled by mCherry (Cre
104 negative) or eGFP (Cre expressing) interspersed in the SuM. We verified the combinatorial viral
105 selectively labeled SuM$^{VGLUT2+}$::POA neurons with minimal background[33]. As positive controls,
106 we injected Retro-AVV-Flpo into the POA and AAV-fDIO-Cre into the SuM to label the cells in
107 SuM (**Supplement Figure 3 G and H**). As negative controls, we injected only AVV-fDIO-Cre into
108 the SuM in Ai14 mice, which did not yield tdTomato expression (**Supplemental Figure 3C-D).** To
109 confirm that the combination of Retro-AAV2-fDIO-Cres and AAV5-DIO-ChR2eYFP did not lead
110 to labeling of cells with eYFP in the absence of Flp, we injected Retro-AAV2-fDIO-Cre into the
111 POA and AAV-DIO-hChR2eYFP into SuM of WT mice. In these mice we did not observe any
112 expression of eYFP (**Supplemental Figure 3E-F**). The results demonstrate the specificity of our
113 combinatorial viral strategy. All studies were replicated in a minimum of three mice.

114 **SuM$^{VGLUT2+}$::POA neurons are an anatomical distinct subset of all SuM$^{VGLUT2+}$ neurons.**

115 Recent studies have highlighted functionally divergent roles of SuM neurons and
116 suggested differential projections, particularly to regions of hippocampus and PVT, may identify
117 functionally distinct populations [19, 20]. To examine if SuM$^{VGLUT2+}$::POA neurons are a subset of
118 SuM$^{VGLUT2+}$ neurons, we qualitatively compared the projections of total SuM$^{VGLUT2+}$ neurons to
119 SuM$^{VGLUT2+}$::POA neurons. Similar to projections for SuM$^{VGLUT2+}$::POA neurons (**Figure 1**), we
120 observed labeled projections from the total SuM$^{VGLUT2+}$ neurons in the POA, PVT, IHB, and the
121 CA2 field of the hippocampus (**Figure 2 A-E**). Importantly, we found areas that received
122 projections from the total SuM$^{VGLUT2+}$ and not from SuM$^{VGLUT2+}$::POA neurons. As schematized
123 (**Figure 2K**), projections from the total SuM$^{VGLUT2+}$ but not SuM$^{VGLUT2+}$::POA populations were
124 present in dentate gyrus (DG) and medial habenula (mHb) (**Figure 1G and Figure 2 F-J**).
125 Connection of the SuM to the dentate gyrus is well described and seen here for the SuM$^{VGLUT2+}$

126 population[34-38]. The lack of projections from SuM$^{VGLUT2+}$::POA neurons to dentate gyrus, but
127 not to other structures is a notable difference (**Figure 2J**). Thus, the SuM$^{VGLUT2+}$::POA population
128 represents a subset of the total SuM$^{VGLUT2+}$ neuronal population with distinct projection targets.

129 **Threatening stressors but not spontaneous higher velocity movement recruits**
130 **SuM$^{VGLUT2+}$::POA neurons**

131 Neurons in SuM can be activated by acute stressors, and we sought to examine the
132 recruitment of SuM$^{VGLUT2+}$::POA neurons by threatening stressors [14, 39, 40]. We found that
133 forced swimming induced cFos expression in SuM. Labeling SuM$^{VGLUT2+}$::POA neurons using
134 Retro-AAV-DIO-mCherry revealed an increase in the number of mCherry and cFos labeled cells
135 following forced swim (**Supplemental Figure 4A-G**). To further examine recruitment of
136 SuM$^{VGLUT2+}$::POA neurons by acute stressors, we tested a diverse set of acute threatening
137 stressors using *in vivo* Ca^{2+} detection via fiber photometry. We expressed GCaMP7s in
138 SuM$^{VGLUT2+}$::POA neurons (**Figure 3A-B**) using the combinatorial viral genetic approach detailed
139 for anatomic studies. We developed a dunk assay that utilized a moveable platform allowing mice
140 to be placed into and removed from the water while obtaining fiber photometry recordings. Mice
141 were dunked by lowering the platform below the water level forcing mice to swim for a 30-second
142 trial every 2 minutes for a total of 10 trials (n=8 mice). During the 30-second swim time, mice
143 exhibited active swimming and climbing behaviors reflected in the quantification of mean time
144 mobile approaching 100 percent during the swim period without evidence for a shift in the
145 behavioral strategy (**Supplemental Figure 4I**). These data show repeated exposure to an acute
146 stressor, dunk in water, evoked active coping behavior (time mobile). A 95%, 99%, and 99.9%
147 confidence interval (CI) were calculated to analyze the difference in the Ca2+-dependent signal
148 preceding and subsequently after the dunk. Analysis of Ca^{2+}dependent (470 nm excitation) and
149 isosbestic control (415 nm excitation) signals from fiber photometry recordings revealed a
150 significant (99.9% CI) rapid rise of approximately 5 standard deviations in GCaMP Ca^{2+}
151 dependent signal with start of the swim trial that was sustained through the 30-sec swim period.
152 The Ca^{2+}dependent signal returned to baseline when the platform was raised, removing the
153 animal from the water (**Figure 3F and G**). Repeated exposure to an acute stressor evoking active
154 coping behaviors robustly recruited SuM$^{VGLUT2+}$::POA neurons.

155 To examine additional stressors, we tested a foot shock paradigm (**Figure 3D**) and a
156 predator ambush assay (**Figure 3E**). In foot shock assays, VGLUT2-Flp mice (n=6), prepared as
157 above (**Figure 3A and B**), were subjected to five pseudorandomly spaced trials with a 30 second
158 tone preceding a two-second shock. We observed a significant rapid increase in the Ca^{2+}

159 dependent GCaMP7s signal following the foot shock (99.9% CI; **Figure 3H and I**). For the
160 predator ambush, we adapted a previously demonstrated paradigm using a mock mechanical
161 spider attack [41]. In this assay a remote-controlled mechanical spider was hidden in a box with
162 a swing door. The box was inside a larger walled arena. Mice were able to freely explore the
163 arena, and at a moment when the mouse was in proximity to the box opening, the spider was
164 moved out towards the mouse. The mice fled, often to a corner, stopped, and turned to face the
165 spider (**Supplemental video 1**). In mice (n=9) subjected to the ambush paradigm, we observed
166 a significant (99.9% CI) increase in Ca^{2+} dependent GCaMP signal at the time of the ambush
167 followed by suppression below the initial baseline (**Figure 3J**). Populations of neurons in SuM
168 have previously been found to correlate with future movement velocity [42], so we examined if
169 recruitment of $SuM^{VGLUT2+}$::POA neurons was correlated to periods of spontaneous higher velocity
170 movement. Analyzing data collected prior to the ambush event, we examined if increased velocity,
171 at speeds similar to the fleeing induced by the ambush, was correlated with increased Ca^{2+}
172 dependent GCaMP signal in $SuM^{VGLUT2+}$::POA neurons (**Figure 3L**). We found no correlation
173 (**Figure 3K**). We further examined the data for a correlation of increased Ca^{2+} dependent signal
174 in $SuM^{VGLUT2+}$::POA neurons to movement velocity during open field exploration in a sperate
175 cohort of mice (n=13). Here, we found no evidence for correlation of velocity with Z-score of Ca^{2+}
176 dependent signal including a cross correlation analysis to account for a potential temporal offset
177 (**Supplemental Figure 5**). In aggregate, the data support recruitment of $SuM^{VGLUT2+}$::POA
178 neurons by diverse threatening stressors but not during times of higher velocity spontaneous
179 movement.

180 **$SuM^{VGLUT2+}$::POA neurons evoke active coping-like behaviors**

181 To examine how activation of $SuM^{VGLUT2+}$::POA neurons contributes to responding to
182 threatening stressors, we assessed behavioral changes evoked by photostimulation of
183 $SuM^{VGLUT2+}$::POA neurons. We injected VGLUT2-Cre or WT (Cre- littermates) mice with Retro-
184 AAV5-DIO-ChR2eYFP in the POA, and an optic fiber was placed over SuM (**Figure 4A**). We
185 employed a paradigm with a 15-minute trial divided into three 5-minute periods: pre-stimulation,
186 stimulation at 10 Hz, and post-stimulation. Based on review of videos obtained during the 15-
187 minute trials, we observed behaviors that could be classified into nine distinct categories:
188 grooming, immobile, walking, chewing of bedding, rearing, rapid locomotion (movement was
189 limited by the size of the arena), digging (moving bedding towards the tail), treading (moving
190 bedding forward with front paws), and jumping (**Figure 4B**). A blinded observer scored the
191 behaviors in 10-second intervals for the predominant behavior observed during each interval, and

each behavior was assigned a color for visualization. Color coded representation of trials from 16 Cre+ (n=16) and WT (n=16) mice is illustrated (**Figure 4B**). The behavioral pattern in the pre-stimulation period is similar between the Cre+ and WT mice. During the stimulation period, a clear shift in behavior was evident in Cre+ mice. Photostimulation induced rearing, treading, digging, rapid locomotion, and jumping. During the post-stimulation period we observed a new pattern with Cre+ mice spending time immobile and grooming. An example of a Cre+ animal is shown in **Supplemental video 2**.

We analyzed behavior, quantifying specific behaviors during each period. Quantification of jumping revealed that Cre+ mice (n=16) engaged in significantly ($p=0.012$) more jumps during the stimulation period compared to WT (n=16) mice (**Figure 4C**). During the pre- and post-stimulation periods, there was not a significant difference in the number of jumps (pre-stimulation = $p>0.999$ and post-stimulation = $p>0.999$). We also observed that during the stimulation period the Cre+ mice engaged in bouts treading/digging, vigorously moving bedding forwards and backwards, as previously described for defensive burying [43]. Defensive burying, characterized by moving bedding forward or backwards often in alternating pattern, is evoked by threatening and noxious stimuli, and is a described active stress coping strategy in rodents[43-46]. We conservatively quantified together the movement of bedding as treading/digging that may include spontaneous digging (**Figure 4D**) and found no significant ($p=0.95$) difference during the pre-stimulation period. In the stimulation period, there was a significant ($p=0.004$) increase in the time spent treading/digging, and, surprisingly, during the post-stimulation period time treading/digging was significantly ($p=0.014$) decreased in Cre+ mice. The variability in behaviors can be attributed to exclusion of one behavior by the other, with individual mice having variability in the predominant behavior displayed during the photostimulation period, but all mice shifted to increased active coping behaviors. The behaviors evoked by photostimulation fit with active coping behaviors seen in the context of stressors. Specifically, escape (jumping, rapid locomotion), defensive burying/treading (digging, pushing beading forward).

We also quantified grooming behaviors in each of the three periods (**Figure 4E**). During the pre-stimulation period, there was not a significant difference ($p>0.999$). During the stimulation period, the Cre+ mice did not engage in grooming, leading to a significant ($p=0.016$) decrease in time spent grooming compared to Cre- mice. In the post-stimulation period, Cre+ mice showed a significant ($p=0.005$) increase in time spent grooming compared to Cre- mice. A reasonable interpretation of the rise in grooming post stimulation is that photostimulation evoked a stressed-like state and cessation of photostimulation led to selfcare grooming, as seen following acute stressors [47, 48]. In summary, the analysis of behaviors elicited by photostimulation of

226 SuM$^{VGLUT2+}$::POA neurons without conditioned cues or concomitant stressors demonstrates a
227 dramatic shift in behavior to escape oriented (jumping, rapid locomotion) and threat response
228 behavior, including rearing and defensive burying, during the photostimulation period. In contrast
229 to freezing, the behaviors elicited by activation of SuM$^{VGLUT2+}$::POA neurons indicate that they
230 may promote active coping strategies.

231 **Photostimulation of SuM$^{VGLUT2+}$::POA neurons drives real-time avoidance**

232 To examine whether activation of SuM$^{VGLUT2+}$::POA neurons may contribute to the aversive
233 aspects of threatening stress, we carried out real-time place aversion testing (RTPA) by pairing
234 one side of the chamber with photostimulation of SuM$^{VGLUT2+}$::POA (**Figure 5A**) neurons at
235 multiple frequencies (1,5,10, and 20 Hz). Photostimulation of SuM$^{VGLUT2+}$::POA neurons produced
236 significant aversion at all frequencies in Cre+ (n=19) mice compared to Cre- (n=21) littermate
237 control mice, and higher stimulation frequencies evoked greater aversion ($p<0.001$; **Figure 5B**
238 **and C**). Example of Cre+ mice with stimulation at 1, 5, and 10Hz as well as Cre- mice is in
239 **Supplemental Video 3**. WT and Cre+ mice explored equivalently, with similar number of entries
240 to the stim side ($p= 0.41$; **Figure 5D**). Cre+ mice quickly left the stimulation side, and the average
241 time spent on the stimulation side of the area was significantly lower ($p<0.001$**; Figure 5E**). These
242 data indicate, surprisingly, that photostimulation, although aversive, did not generate aversive
243 pairing, as found for other brain areas [49]. To examine the relative aversiveness of
244 SuM$^{VGLUT2+}$::POA photostimulation, we carried out RTPA experiments using an arena with a dark
245 side and a bright side (**Figure 5F inset**). We paired photostimulation with the dark side. As
246 expected, Cre- mice show a preference for the dark side of the arena, however, photostimulation
247 of the SuM$^{VGLUT2+}$::POA neurons yielded significant aversion of Cre+ (n=13) compared to Cre-
248 (n=12) ($p<0.001$; **Figure 5F)**. Cre+ mice spent nearly the entire trial in the brightly lit side,
249 demonstrating photostimulation of SuM$^{VGLUT2+}$::POA neurons drove avoidance sufficient to
250 overcome a mildly aversive stimulus (bright light).

251 Reports have described multiple populations of neurons in supramammillary including
252 populations that project to the dentate gyrus of the hippocampus that release both GABA and
253 glutamate. Our anatomic studies indicated that SuM$^{VGLUT2+}$::POA neurons do not project to the
254 dentate gyrus (**Figure 2**) and are not GABAergic (**Supplemental Figure 1G-L**). Thus,
255 SuM$^{VGLUT2+}$::POA neurons are not part of either a GABAergic or dual transmitter population. To
256 examine if GABAergic neurons in SuM (SuM^{VGAT+}) can mediate real-time place aversion or
257 preference, we injected VGAT-Cre mice with AAV to express ChR2 (n=26) or control (n=26) in
258 SuM and carried out real-time place aversion testing. Photostimulation at 10 Hz yielded no

259 significant aversion or preference compared to baseline (p=.838) (**Supplemental Figure 6A-D**).
260 This is in contrast to the robust aversion caused by photostimulation of SuM$^{VGLUT2+}$::POA neurons.

261 **Photoactivation of SuM$^{VGLUT2+}$::POA neurons does not cause anxiogenic-like behavior**

262 Threat can induce anxiety-like, risk aversion behavioral states [50-52]. To test whether
263 activity of SuM$^{VGLUT2+}$::POA neurons contributes to anxiety-like behaviors, we used two
264 established assays for anxiety-like behavior: open field and light-dark exploration [53-56]. During
265 open field testing, 10 Hz photostimulation was applied to SuM$^{VGLUT2+}$::POA neurons. We quantified
266 the time spent in the perimeter (outer 50%) vs. the center (inner 50%) of the arena and found
267 VGLUT2-Cre+ (n=18) and WT (n=17) mice did not significantly differ (center p=0.17 and perimeter
268 p=0.19; **Figure 5G and H**). The total distance traveled was significantly (p<0.001) increased in in
269 Cre+ mice compared to WT mice (**Figure 5I**). Increased distance traveled in some mice was not
270 surprising, because prior testing (**Figure 4**) revealed the mice engaged in escape behaviors
271 during photostimulation. We observed behaviors including jumping during open field testing as
272 well. We also carried out open field testing using VGAT-Cre mice to selectively activate SuM^{VGAT+}
273 neurons and observed no significant effect on time in center (p=0.254) or perimeter (p=0.287)
274 (**Supplemental Figure 6F**), but mice expressing ChR2eYFP displayed a small but significant
275 (p=0.035) decrease in distance traveled **(Supplemental Figure 6G)**. We tested if
276 photostimulation of SuM$^{VGLUT2+}$::POA neurons would increase preference for the dark area, a
277 potential sign of elevated anxiety (**Figures 5J**). We found that photostimulation of
278 SuM$^{VGLUT2+}$::POA neurons did not significantly alter preference (p=0.68; **Figure 5K**) in VGLUT2-
279 Cre+ mice (n=8) compared to WT (n=9). The activation of SuM$^{VGLUT2+}$::POA neurons evoked
280 escape behaviors in open field testing, as seen in Figure 4; similarly, a significant increase in total
281 distance was detected during light-dark exploration assay in Cre+ compared to WT (p=0.003;
282 **Figure 5L**). The findings we obtained in open field and light-dark exploration testing do not support
283 a role for SuM$^{VGLUT2+}$::POA neurons in driving anxiety-like behaviors.

284 **SuM$^{VGLUT2+}$::POA neurons can drive instrumental action-outcome behavior**

285 Current theoretical frameworks for examining threat responses divide behaviors into two
286 broad categories: innate (fixed) and instrumental (action-outcome)[1, 57]. Additionally, stress
287 responses can be divided into active vs passive actions. Behaviors in these separable categories
288 are mediated by distinct neural circuits[1, 58]. For example, areas involved in responding to
289 specific threatening stimuli (looming threat) drive an innate fixed behavior repertoire[10].
290 Photostimulation of SuM$^{VGLUT2+}$::POA neurons evoked multiple active-like behaviors in response
291 to threatening or noxious stimuli (**Figure 4**). To test if SuM$^{VGLUT2+}$::POA neurons can promote

292 flexible repertoires of behavior including instrumental tasks, as opposed to only innate behaviors
293 (ex. fleeing), we used an operant negative reinforcement paradigm (**Figure 6A-B**). Because our
294 results show photostimulation of $SuM^{VGLUT2+}$::POA neurons is aversive, photostimulation of
295 $SuM^{VGLUT2+}$::POA neurons could be used as a negative reinforcer in a negative reinforcement
296 paradigm. We employed a paradigm using two nose poke ports, one active and one inactive.
297 $SuM^{VGLUT2+}$::POA neurons were photostimulated at 10 Hz during a 10-minute trial. Activation of
298 the active port by a nose poke triggered a 10-second pause in photostimulation of
299 $SuM^{VGLUT2+}$::POA neurons and turned on a house light for 10 s (**Figure 6A and B**). Following this
300 10-second pause, the house light switched off and photostimulation resumed until the subsequent
301 activation of the active port. We tested animals for four consecutive days with the 10-minute trials
302 without prior training. Importantly, performance of the task had to be completed during
303 photostimulation.

304 We hypothesized that if stimulation of $SuM^{VGLUT2+}$::POA evokes fixed innate defensive
305 behaviors, or simply promotes high amounts of locomotion, then performance of an operant task
306 (an action-outcome behavior) with active and inactive ports would be impaired because innate
307 defensive behaviors would conflict with performance of the operant task. Importantly, results
308 obtained can help differentiate general elevation in locomotor activity from directed coping
309 behavior. Analyses of port activations during the 10-minute trials revealed that Cre+ mice (n =11)
310 paused the photostimulation (reward) significantly more on all four days of testing compared to
311 Cre- littermate (n=11) mice ($Interaction_{Genotype\ x\ Day}$ $p<0.001$; Day 1 $p<0.001$; Day 2 $p<0.001$; Day
312 3 $p<0.001$; Day 4 $p<0.001$; **Figure 6C**). The number of 10-second pauses approached the
313 maximum, 60 possible in a 10-min period. Cre+ mice engaged the active port significantly more
314 than Cre- mice ($p<0.001$; **Figure 6D**) and this effect was consistent for every training session
315 (Day 1 $p<0.0001$=; Day 2 $p<0.0001$; Day 3 $p<0.0001$; Day 4 $p=0.0011$). There was a slight
316 difference in baseline performance of the task. The time to the first engagement of the active port
317 was significantly different for Cre+ compared to Cre- mice during the first test trial ($p=0.046$).
318 During the three subsequent tests, Cre+ mice were significantly faster to engage the active port
319 after the start of the trial compared to Cre- mice (Day 2 $p=0.009$; Day 3 $p=0.003$; Day 4 $p=0.034$;
320 **Figure 6E**). Cre+ mice engaged the active port significantly more than the inactive port on all test
321 days ($p<0.001$; **Supplemental Figure 7A**). There was not a significant difference in Cre+ and
322 Cre- mice for engagement of the inactive port on any day (Cre+ $p=0.30$; Cre- $p=0.055$;
323 **Supplemental Figure 7A-B**).Furthermore, Cre+ mice were significantly faster in the second
324 through fourth trials at engaging the active port compared the first trial (Day 1 vs Day 2 $p=0.034$;

325 vs Day 3 p=0.021; vs Day 4 p=0.027; **Figure 6E**). Suggesting that mice became more proficient
326 during subsequent trials.

327 To examine effort-related motivation, we employed a 30-minute test using a progressive
328 ratio requiring an exponentially increasing number of active port activations to trigger a pause in
329 the photostimulation on the fifth day of operant behavior testing **(Figure 6B**) [59]. During trials
330 using a progressive ratio, Cre+ mice activated the active port and paused stimulation significantly
331 ($p<0.001$) more times than Cre- mice (**Figure 6F**). Examination of individual cumulative active
332 port activation data showed Cre+ mice continued to engage the active port throughout progressive
333 ratio trials despite the increasing work required to generate each pause in photostimulation. No
334 breakpoint was observed during the trial (**Figure 6G and H**). This finding indicates that activation
335 of $SuM^{VGLUT2+}$::POA neurons remains salient and motivating through the tested period and that
336 photostimulation of $SuM^{VGLUT2+}$::POA does not evoke behaviors precluding completion of the task.
337 Examination of reward behavioral epochs for representative animals shows that for the lowest
338 total number of rewards earned (green dots), the next pause required 20 activations of the active
339 port, and for the highest (red dots), the next pause required 50 activations of the active port. Taken
340 together, results from the instrumental reinforcement tasks demonstrate that activation of
341 $SuM^{VGLUT2+}$::POA neurons does not solely evoke innate stereotyped behaviors and can drive
342 active coping in the form of instrumental behaviors.

343 **$SuM^{VGLUT2+}$::POA neurons are recruited during active coping behaviors during forced swim**

344 The forced swim test is increasingly established as an assay of coping strategy with
345 passive and active components, and we used forced swim testing in conjunction with fiber
346 photometry to examine if $SuM^{VGLUT2+}$::POA neurons are recruited differentially during active
347 (mobile) or passive (immobile) behaviors [60, 61]. During a first 15-mintute trial of forced
348 swimming, mice shifted from active escape behaviors (wall climbing, robust swimming) to passive
349 (immobile floating) behaviors. We carried out experiments using fiber photometry paired with
350 automated computer-based behavior analysis [62]. The automated behavior scoring enabled high
351 temporal resolution analysis of behaviors (**Supplemental Video 4**) and each frame of the video
352 was coded for the classified behavior and plotted as a color-coded point. We observed four types
353 of behavior during forced swimming: climbing, swimming, hindpaw swimming, and immobile
354 floating, and we trained a model to identify each. Analysis of behavior showed that after the first
355 minutes of the trial, mice shifted from swimming and climbing to immobile floating with intermittent
356 swinging or hindpaw swimming. We analyzed fiber photometry recordings to examine whether
357 recruitment of $SuM^{VGLUT2+}$::POA neurons changed with this shift to more passive behaviors. As

358 shown in the representative trace (**Figure 7A**), the Ca^{2+}-dependent signal, but not the isosbestic
359 signal, markedly decreased at the time the shift in behavior was occurring. To combine behavioral
360 data, we assigned numerical values, one through four, to each behavior: climbing (4), swimming
361 (3), hindpaw swimming (2), and immobile floating (1). The mean was plotted as a heat map (red
362 higher values to blue lower values) to be compared to time locked fiber photometry data (**Figure**
363 **7B**). Examining the timeframe around the behavioral shift in each animal, we found that as
364 behavior shifted from active coping (climbing, swimming) to more passive strategies and greater
365 immobility, the Ca^{2+} signal significantly (95% CI) declined (**Figure 7B**). Examining the data after
366 this initial transition, we observed that many elevations in the Z-score were accompanied by
367 changes in behavior to swimming or hindpaw swimming (**Figure 7A**). To further examine this
368 possible correlation, we examined the time frame around transition to hindpaw swimming for
369 changes in Ca^{2+} signal. In a 20-second window centered on the onset of hindpaw swimming, we
370 found that hindpaw swimming was accompanied by a rise in the Ca^{2+} dependent signal across
371 multiple events within a trial (**Figure 7C**). A similar analysis across events in multiple animals
372 demonstrated a significant (99.9% CI) rise in the Ca^{2+} dependent signal from $SuM^{VGLUT2+}$::POA
373 neurons during the shift from immobility to hindpaw swimming or swimming behaviors (**Figure**
374 **7D**). Time series analysis of 20-second epochs centered on random time intervals did not reveal
375 any rise in the Ca^{2+} dependent signal (**Figure 7E**). These data indicate that recruitment of
376 $SuM^{VGLUT2+}$::POA neurons fluctuates with changes in coping strategy during a forced swim assay
377 with decreased engagement of this circuit during times of immobility.

378 **$SuM^{VGLUT2+}$::POA neurons promote active coping during forced swim test**

379 We found that $SuM^{VGLUT2+}$::POA neurons are activated by acute stressors (**Figure 3**) and
380 are recruited during times of greater active coping behaviors (**Figure 7**). To test if
381 $SuM^{VGLUT2+}$::POA neurons can drive a switch in coping strategy in the context of ongoing
382 stressors, we used a two-day forced swim stress test [61, 63]. We tested animals during the
383 second day, when immobile floating is the predominant behavior. As in previous experiments, we
384 used VGLUT2-Cre (Cre+) or WT (Cre-) mice injected in the POA bilaterally with Retro-AVV-DIO-
385 ChR2eYFP. On day one, we subjected mice to 15 mins of forced swim. On the subsequent day,
386 we repeated the forced swim for 6 mins divided into three periods: pre-stimulation, stimulation at
387 10Hz, and post-stimulation (**Figure 7F**). Trials on the second day were recorded and scored by a
388 blinded observer for time spent immobile in each 2-minute period. An example of a Cre+ mouse
389 with stimulation 10Hz is shown in **Supplemental Video 3**. During the pre-stimulation period, there
390 was not a significantly ($p>.999$) different amount of time immobile between Cre+ ($n=9$) and Cre-

391 (n=11) mice. During the stimulation period, Cre+ mice began swimming and attempting to climb
392 the wall of the circular swim arena, reflected by significantly ($p<0.001$) less time immobile (**Figure**
393 **7H**). Interestingly, in the post stimulation phase, the difference in time spent immobile between
394 Cre+ can WT mice decreased but remained significantly ($p=0.047$) different. These results
395 indicate that in the context of an ongoing stressor, activation of $SuM^{VGLUT2+}$::POA neurons is
396 sufficient to trigger a change in coping strategy from largely passive (floating) to active (swimming,
397 climbing). The persistent effect of the acute activation into the poststimulation phase suggests
398 that activation of $SuM^{VGLUT2+}$::POA neurons may shift how the stressor is processed or
399 approached.

400 We next examined the effect of 10 Hz photostimulation of SuM^{VGAT} neurons on coping
401 strategy using the same two-day swim paradigm. VGAT-Cre mice were injected in the SuM to
402 express ChR2eYFP (n=10) or control (eYFP) (n=11), and a fiber optic was placed over SuM
403 (**Figure 7F**). Quantification of behavior revealed no significant difference in time spent immobile
404 during the pre-stimulation ($p=.218$) or the stimulation ($p>.999$) periods. Surprisingly, in the post-
405 stimulation period, we observed a dramatic shift in behavior, marked by a significant ($p=0.047$)
406 decrease in time spent immobile (**Figure 7I**). The amplitude of change in behavior was similar to
407 what we observed during the stimulation phase of the experiments on $SuM^{VGLUT2+}$::POA neurons
408 (**Figure 7H**). One interpretation of these data is that release of sustained local inhibition leads to
409 rebound activity of output $SuM^{VGLUT2+}$::POA neurons.

410 **Suppression of $SuM^{VGLUT2+}$::POA neurons is required for feeding**

411 Feeding and responding to threats are conflicting actions, and $SuM^{VGLUT2+}$::POA neurons
412 may play a role in switching between behavioral paradigms (e.g., feeding vs escape). We sought
413 to examine $SuM^{VGLUT2+}$::POA neuron activity in relation to feeding using fiber photometry based
414 GCaMP recordings. To promote differential drive for food, mice were given *ad lib* access to food
415 (fed condition) or food deprivation for 24 hours, and on testing day, were presented with a chow
416 pellet, while Ca^{2+} dependent GCaMP fluorescence and isosbestic signals were recorded. In the
417 fed state, mice spent significantly less time interacting with the food ($p<0.001$; **Figure 8C**) and ate
418 significantly less ($p<0.001$; **Figure 8D**) compared to food deprived state. We analyzed the Ca^{2+}
419 dependent and isosbestic signals around presentation of food to fed and food deprived mice. In
420 the food deprived state, mice spent more time with the food and ate more food (**Figure 8E and**
421 **F**). At the time of food presentation, the Ca^{2+} dependent signal decreased significantly (99.9% CI)
422 but not the isosbestic signal. The change in the Ca^{2+} dependent signal was larger and more
423 sustained when the animals spent longer interacting with the food (**Figure 8E and F**). Together,

424 the data support suppression of SuM$^{VGLUT2+}$::POA neural activity during consummatory behavior
425 with greater consumption associated with enhanced suppression.
426 To examine whether activation of SuM$^{VGLUT2+}$::POA neurons disrupted consummatory
427 behavior, we tested the impact of photostimulation on feeding behavior in food deprived mice.
428 Using VGLUT2-Cre (Cre+) or WT (Cre- littermates) mice injected with Retro-AAV2-DIO-
429 ChR2eYFP into the POA and implanted with a fiber optic midline over SuM, we examined how
430 feeding behaviors in food deprived mice were altered by 10 Hz photostimulation of
431 SuM$^{VGLUT2+}$::POA neurons (**Figure 8G-I**). We used trials lasting 20 mins with unrestricted access
432 to food added at the start of the trial. Each trial was divided into three periods: a 5-min pre-
433 simulation period, 10-min stimulation period, and a 5-min post-stimulation period. Trials were
434 recorded and scored for time spent interacting with the food pellet. During the pre-stimulation
435 period, Cre+ (n=17) and Cre- (n=16) mice spent interacting with the food was not significantly
436 different ($p>0.999$). Upon the introduction of photostimulation, the Cre+ mice stopped eating and
437 interacting with the food. During the photostimulation period, Cre+ mice spent significantly less
438 time interacting with the food compared to Cre- mice ($p<0.001$). Surprisingly, the decrease in time
439 spent interacting with food continued into the post-stimulation phase, where Cre+ mice continued
440 to interact with the food significantly less than Cre- mice ($p<0.001$; **Figure 8H**). Reflecting the
441 decrease in time spent with the food, Cre+ mice consumed significantly less food during the 20-
442 min trial than Cre- mice ($p=0.001$; **Figure 8I**). These results indicate that SuM$^{VGLUT2+}$::POA
443 neurons can redirect behavior away from consumption, and suppression of SuM$^{VGLUT2+}$::POA
444 neurons is required for feeding, even in a food deprived state. Ethologically, animals must choose
445 rapidly between responding to threats and feeding when foraging. The findings here implicate this
446 pathway in control of switching between these behaviors.

447 **Discussion**

448 Together, the presented data show SuM$^{VGLUT2+}$::POA neurons function as a hub, with
449 connections to many brain areas, to regulate responses to threatening stressors. We report here
450 that SuM$^{VGLUT2+}$::POA neurons have broad arborizations to multiple brain regions involved in
451 responding to threat and stress (**Figures 1, 2, and Supplemental Figure 2**). We identified diverse
452 threatening stressors (dunk, shock, and predator), which elicit differential behavioral responses,
453 swimming, jumping, and fleeing, recruit SuM$^{VGLUT2+}$::POA neurons. Using a forced swim test, we
454 found that recruitment of SuM$^{VGLUT2+}$::POA neurons is correlated with periods of spontaneous
455 active coping (swimming, climbing) and not with passive (immobile) behaviors. These data
456 collectively indicate that SuM$^{VGLUT2+}$::POA neurons are recruited by threatening stressors,

457 preferentially during active coping. We also examined the roles of SuM$^{VGLUT2+}$::POA neurons in
458 responding to stressors by stimulating SuM$^{VGLUT2+}$::POA neurons, and selective activation of
459 SuM$^{VGLUT2+}$::POA neurons evoked active coping-like behaviors in the absence of a stressor
460 (**Figure 4**). SuM$^{VGLUT2+}$::POA neuron activation drove aversion but did not promote anxiety-like
461 behaviors (**Figure 5**). We also used a negative reinforcement test, requiring selective activation
462 of an active port over the inactive port to show SuM$^{VGLUT2+}$::POA neurons can drive flexible, in
463 contrast to fixed or reflexive, behaviors (**Figure 6**). Activation of SuM$^{VGLUT2+}$::POA neurons
464 increased active coping during ongoing stress in a forced swim assay (**Figure 7H**). Finally,
465 examining the conflicting behaviors required for threat response and feeding, we found
466 SuM$^{VGLUT2+}$::POA neurons were suppressed during feeding and that activation of
467 SuM$^{VGLUT2+}$::POA neurons blocked feeding activity (**Figure 8**). Thus, SuM$^{VGLUT2+}$::POA neurons
468 contribute to affective component of stress, promote active coping behaviors, and shift behavior
469 to shift threat responsivity away from feeding.

470 The presented results demonstrate SuM$^{VGLUT2+}$::POA neurons act as a distinct subset of
471 neurons projecting to many but not all areas receiving projections from the total SuM$^{VGLUT2+}$
472 population. Notably, mHb and DG projections were present in the SuM$^{VGLUT2+}$ population but
473 absent in the SuM$^{VGLUT2+}$::POA projections (**Figure 3K**), consistent with a separation of DG and
474 CA2 projecting SuM neurons [64]. The extensive arborization of SuM$^{VGLUT2+}$::POA neurons
475 challenges the often-employed neural circuit concept that projection from a single area to a
476 another area mediates or modifies a behavior. The projections to PVT, Hb, and PAG are of
477 particular interest because these areas regulate stress coping [65-68]. Dopamine receptor 2
478 expressing neurons in the PVT have been implicated in promoting active coping behaviors and
479 may be a potential target of SuM$^{VGLUT2+}$::POA neurons [8, 9]. The habenula also regulates active
480 vs passive coping behaviors, and the lHb functions in aversive processing, making the selective
481 projections of SuM$^{VGLUT2+}$::POA neurons to the lHb of similar interest [65, 69-72]. In addition, the
482 PAG, which receives projections from SuM$^{VGLUT2+}$::POA neurons, has been implicated in
483 regulating defensive behaviors and coping strategies [66, 67, 73]. The arborization to these and
484 other areas position SuM$^{VGLUT2+}$::POA neurons to be a central hub for regulating behavioral
485 responses to threatening stressors by concurrent recruitment of multiple areas. Understanding
486 the roles of individual projections in contributing to the overall behavioral response will require
487 further studies.

488 Superficially, the aversiveness of SuM$^{VGLUT2+}$::POA neuron stimulation we report contrasts
489 with a recent study that found photostimulation of SuM neuron projections could be reinforcing.
490 Photostimulation of projections from SuM to the septum drove place preference (septum), but the

491 same report found photostimulation of SuM projections in the PVT was aversive[19]. We report
492 here that SuM$^{VGLUT2+}$::POA neurons also project to the PVT and the septum (**Figure 2**). A plausible
493 interpretation is that SuM contains separable, molecularly defined populations of neurons which
494 gate a host of distinct behavioral strategies through their connectivity and/or co-transmitter
495 content. Delineating the overarching circuitry will require further in depth studies, but our results
496 together with recent studies establish the SuM as an important and poorly understood node which
497 regulates both appetitive and aversive motivated behavior.

498 We addressed the challenge of potential confounds from locomotor activity inherent in
499 active coping behaviors, which is of special concern here because a population of SuM neurons
500 have been found to correlate with velocity of movement. To do so we used multiple behavioral
501 assays together with fiber photometry and photostimulation. We found multiple threatening
502 stressors (dunk, shock, ambush) with differing evoked behaviors all recruit SuM$^{VGLUT2+}$::POA
503 neurons (**Figure 3**). We also found increased recruitment of SuM$^{VGLUT2+}$::POA neurons during
504 active coping behaviors (**Figures 3 and 7**). We did not find evidence for recruitment of
505 SuM$^{VGLUT2+}$::POA neurons during elevated locomotion in two cohorts in assays of free movement
506 (**Figure 3K-M and Supplemental Figure 5**). These data are in contrast to recent studies that
507 found activity of some neurons in SuM correlated future velocity [42]. We carefully examined the
508 behaviors elicited by activation of SuM$^{VGLUT2+}$::POA neurons both in absence of stressors (**Figure**
509 **4**) and during ongoing stressors (**Figure 7**) and found that stimulation of SuM$^{VGLUT2+}$::POA
510 neurons promoted active coping behaviors, which involved increased physical activity. We
511 examined if SuM$^{VGLUT2+}$::POA neurons could also drive performance of an operant task which
512 would be impaired if activation of SuM$^{VGLUT2+}$::POA neurons lead to fixed escape behaviors. We
513 found that the mice effectively performed the operant task, extensively activating the active port,
514 instead of the inactivate port. Taken together, the results from the behavioral tests indicate that
515 SuM$^{VGLUT2+}$::POA promote flexible stressor appropriate coping behaviors and not generalized
516 locomotion.

517 Although neurons in SuM can release both GABA and glutamate in the dentate gyrus, our
518 anatomic studies indicate that SuM$^{VGLUT2+}$::POA neurons were discrete from GABAergic neurons
519 and do not project the dentate gyrus (**Figure 2 and Supplemental Figure2**)[21, 31]. Thus,
520 SuM^{VGAT} neurons could be a functionally distinct population. We tested the effects of
521 photostimulation of SuM^{VGAT} neuron and, in contrast to SuM$^{VGLUT2+}$::POA neurons, found no effect
522 on place aversion, minor decreases in locomotion, and no significant change in active coping
523 behaviors during stress (FST) during stimulation. Surprisingly, immediately after photostimulation
524 stopped, active coping behavior increased dramatically (**Figure 7I**). These data demonstrate

525 functional separation of SuM^{VGAT} and suggest connection between the $SuM^{VGLUT2+}$::POA and
526 SUM^{VGAT+} populations that require further investigation to elucidate.
527 In conclusion, $SuM^{VGLUT2+}$::POA neurons arborize to multiple areas involved in stress and
528 threat response that promote active coping behaviors. Passive coping strategies have been
529 associated with unescapable stress, anhedonia, and depression[7, 74-76]. Targeting
530 neuromodulation of a circuit able to act across many brain areas may represent a therapeutic
531 avenue for common psychiatric conditions, and $SuM^{VGLUT2+}$::POA neurons are a newly identified
532 node in critical approach-avoidance circuitry.

533 **Acknowledgements**

534 This work was supported by the NIH through 5R01MH112355 to MRB and P30DA048736
535 (MRB) and 5K08MH119538 to AJN. Support was also provided by the Hope Center Viral Vectors
536 Core and the Genome Technology Resource Center at Washington University in St. Louis (NIH
537 P30CA91842 and UL1TR000448). This work was supported by a Pilot Project Award from the
538 Hope Center for Neurological Disorders and by the Hope Center Viral Vectors Core at Washington
539 University School of Medicine.
540

541 **Materials and Methods**

542 **Methods**

543 Key Resources Table:

Reagent type (species) or resource	Source or reference	Identifiers
Antibodies		
Alexa Fluor 488 Goat anti-Rabbit IgG	Invitrogen	Cat# A11008
Phospho-c-Fos (Ser32) (D82C12) XP®	Cell Signaling Technology	Cat# 5348
Chemicals		
4% paraformaldehyde	J.T. Baker, Avantor	S898-09
Goat Serum	Sigma Aldrich	G9023
Vectashield Hardset Antifade Mounting Medium with DAPI	Vector Laboratories	Cat# NC9029229
Experimental Models: Organisms/Strains		
Slc17a6tm2(cre)Lowl/J (VGLUT2-Cre)	The Jackson Laboratory	RRID:IMSR_JAX:016963
B6;129S-Slc17a6tm1.1(flpo)Hze/J (VGLUT2-Flp)	The Jackson Laboratory	RRID: IMSR_JAX: 030212
Mouse:B6.Cg-Gt(ROSA)26Sor$^{tm14(CAG-tdTomato)Hze}$/J (Ai14)	The Jackson Laboratory	RRID: IMSR_JAX: 007914
B6J.129S6(FVB)-*Slc32a1*$^{tm2(cre)Lowl}$/MwarJ (VGAT-Cre)	The Jackson Laboratory	RRID: IMSR_JAX: 028862
C57BL/6J	The Jackson Laboratory	RRID: IMSR_JAX: 000664
Bacterial and Virus Strains		
AAV5-EF1a-DIO-hChR2(H134R)-EYFP (2.5 × 10^{13} vg/ml)	Washington University Hope Center Viral Vector Core	N/A
AAV2-Retro-DIO-ChR2-eYFP (2.8 × 10^{12} vg/ml)	Washington University Hope Center Viral Vector Core	N/A
AAV2-retro-FLEX-tdTomato (7 × 10^{12} vg/ml)	Addgene	RRID: Addgene_ 28306-AAVrg
AAV5-DIO-ChR2-eYFP (1.4 × 10^{13} vg/ml)	Washington University Hope Center Viral Vector Core	N/A
AAV2-Retro-EF1a-fDIO-cre (7 × 10^{12} vg/ml)	Addgene	RRID: Addgene_ 121675-AAVrg

AAV5-EF1a-Nuc-flox(mCherry)-EGFP (5.7 × 10^{12} vg/ml)	Addgene	RRID: Addgene_112677-AAV5
Retro-AAV2-EF1a-Nuc-flox(mCherry)-EGFP (7 × 10^{12} vg/mL)	Addgene	RRID: Addgene_ 112677-AAVrg
AAV2-retro-EF1a-DIO-eYFP (3 × 10^{13} vg/ml)	Washington University Hope Center Viral Vector Core	N/A
AAV-retro-EF1a-Flpo (1.02 × 10^{13} GC/mL or 7 × 10^{12} vg/ml)	Addgene	RRID: Addgene_ 55637-AAVrg
AAV9-EF1a-fDIO-cre (2.5 × 10^{13} GC/mL or 1 × 10^{13} vg/ml)	Addgene	RRID: Addgene_121675-AAV9
Retro-AAV2-EF1a-Cre (2.1 × 10^13 GC/mL)	Addgene	RRID: Addgene_55636-AAVrg
AAV9-syn-FLEX-GCaMP7s-WPRE (1.2 × 10^{13} GC/ml)	Addgene	RRID: Addgene_104487-AAV9
AAV5-EF1a-DIO-eYFP (1.8 x10^{13} vg/ml)	Washington University Hope Center Viral Vector Core	N/A
AAV2 retro-Ef1a-DIO-mCherry (4.0 × 10^{12} vg/ml	University of Carolina Vector Core	N/A
Software		
Bonsai	Bonsai-rx.org	N/A
Ethovision	Noldus	N/A
GraphPad Prism	GraphPad Software	N/A
Labgym	https://github.com/umyelab/LabGym	N/A
DeepLabCut	https://github.com/DeepLabCut/DeepLabCut	N/A

For further information regarding reagents and resources, contact Aaron Norris, norrisa@wustl.edu.

Experimental model and subject details

549 Adult (25-35 g, at least 8 weeks of age upon experimental use) male and female VGLUT-
550 Cre (RRID: IMSR_JAX:016963), VGLUT2-Flp (RRID: IMSR_JAX: 030212), Ai14 (RRID:
551 IMSR_JAX: 007908), VGAT-Cre (RRID: IMSR_ JAX: 028862) and C57BL/6J (RRID: IMSR_JAX:
552 000664) mice (species *Mus musculus*) were group housed (no more than five littermates per
553 cage) in a 12 hr:12 hr light:dark cycle room with food and water ad libitum[77]. Cre+ and Cre-
554 littermates were used in the experiments unless otherwise noted. The Washington University
555 Animal Care and Use Committee approved all procedures which adhered to NIH guidelines.

556 Stereotaxic surgery

557 Injections and implantations were done as described previously[78, 79]. Briefly, in an
558 induction chamber, mice were anesthetized (4% isoflurane) before being placed in a stereotaxic
559 frame (Kopf Instruments). Anesthesia was maintained with 2% isoflurane. Mice were then injected
560 unilaterally or bilaterally, depending on the combination of virus(es) used and brain regions
561 injected. A blunt needle Neuros Syringe (65457-01, Hamilton Con.) and syringe pump (World
562 Precision Instruments) were used to perform the injection schemes below. After surgery, a
563 warmed recovery chamber housed the animal while it recovered from anesthesia before being
564 returned to its home cage.

Brain Region /Coordinates	Virus Volume	Virus
SuM (AP -2.7-2.85, ML +0.05, DV -4.3-4.5)	50 - 300 nl	AAV5-EF1a-DIO-hChR2(H134R)-EYFP AAV2-retro-DIO-ChR2-eYFP AAV5-EF1a-Nuc-flox(mCherry)-EGFP AAV9-EF1a-fDIO-cre AAV9-syn-FLEX-GCaMP7s-WPRE AAV5-EF1a-DIO-eYFP
POA, bilateral (AP +0.45, ML ± 0.5, DV -5.35)	50 - 150 nl	AAV2-retro-EF1a-fDIO-cre Retro-AAV2-EF1a-Nuc-flox(mCherry)-EGFP AAV2-retro-EF1a-DIO-eYFP AAV2-retro-EF1a-Flpo AAV2 retro-Ef1a-DIO-mCherry
Septum (AP +0.9, ML +0.3, DV -3.5)	100 nl	AAV2-retro-FLEX-tdTomato
LPAG, unilateral (AP -4.65, ML +0.6, DV -2.85)	100 nl	AAV2-retro-FLEX-tdTomato

Acb, unilateral, (AP +1.4, +0.6 ML, DV -4.75)	100 nl	AAV2-retro-EF1a-DIO-eYFP
PVT, unilateral, (AP -1.5, ML 0.0, DV -2.85)	100 nl	AAV2-retro-EF1a-DIO-eYFP

565

566 Injections were made at a rate of 50 nl/min, with the injection needle being withdrawn 5
567 min after the end of the infusion. Fiber optics for photostimulation or optical fibers for fiber
568 photometry were implanted after injections for all behavioral experiments.
569 Fiber optic implants for photostimulation were fabricated as previously described using
570 200µm glass fibers and implanted midline over SuM [78, 80]. For implantation, the skull was
571 cleaned and etched with OptiBond® (Kerr) and the fiber was cemented to the skull with Tetric N-
572 Flow® (Ivoclar Vivadent). Blue light was used to cure and harden cement. Mice were allowed to
573 recover for at least seven days before the start of behavioral experiments. The same process was
574 used for implantation for fiber photometry fibers, which were purchased from Neurophotometrics
575 and trimmed to length.
576 Anatomical tracing
577 For anterograde viral tracing experiments, virus was injected at least six weeks prior to
578 transcardial perfusions with 4% paraformaldehyde to allow for anterograde transport of the
579 fluorophore. AAV5-EF1a-DIO-hChR2eYFP or AAV5-EF1a-DIO-eYFP were used. Alternatively, to
580 label only $SuM^{VGLUT2+}$::POA neurons for anterograde tracing, Retro-AAV2-DIO-eYFP or Retro-
581 DIO-ChR21eYFP was injected into the POA with AAV-fDIO-Cre injected in the SuM. A minimum
582 of six weeks was allowed prior to sacrifice, harvesting or brains, and sectioning (30µM). Serial 30
583 µM sections approximately 60µM apart were examined. For retrograde studies, viruses were
584 injected (see figure legends and text for specific viruses) at the targeted site and table for specific
585 viruses[81-83]. Three weeks were allowed to elapse prior to harvesting brains following injections.
586 Images were obtained on a Leica DM6 B upright microscope and processed using Thunder
587 imaging station (Leica).
588 Brain clearing and light sheet microscopy
589 Tissue clearing and imaging was carried out on brains collected and fixed in 4% PFA as
590 described above by LifeCanvas Technologies. Briefly, brains were fixed using SHIELD post ix
591 and cleared for seven days in SmartClear II Pro. Index matched with EASYIndex at room
592 temperature. Samples were mounted ventral side up and imaged at 3.6x with pixel size 1.8 x 1.8
593 mm, axial resolution < 4 µm, z step 4 µm in 488nm channel. Fos was labeled by Alexa Flour 488.
594 SuM boundaries were defined by -2.6 to -2.95 rostral to Bregma. The medial mammillary nucleus

595 and the mammillary recess of the 3rd ventricle marked the medial and ventral boundaries, while
596 fornix marked the lateral, and fasciculus retroflexus marked the dorsal boundaries. Images were
597 quantified by a trained laboratory member who was blind to the experimental conditions.

598 Immunohistochemistry

599 Mice were intracardially perfused with 4% PFA and then brains were sectioned (30
600 microns) and placed in 1x PB until immunostaining. Free-floating sections were washed three
601 times in 1x PBS for 10 min intervals. Sections were then placed in blocking buffer (0.5% Triton X-
602 100% and 5% natural goat serum in 1z PBS) for 1 hr at room temperature. After blocking buffer,
603 sections were placed in primary antibody rabbit Phospho-c-Fos (Ser32) antibody (1:500, Cell
604 Signaling Technology) overnight 4 °C temperature. After 3 x 10 min 1x PBS washes, sections
605 were incubated in secondary antibody goat anti-rabbit Alexa Fluor 488 (1:2500, Invitrogen) for 2
606 hr at room temperature. Sections were washed in 1x PBS (3 x 10 min) followed by 2 x 10 min 1x
607 PB washes. After immunostaining, sections were mounted on Super Frost Plus slides (Fisher)
608 and covered with Vectashield Hard set mounting medium with DAPI (RRID:AB_2336788, Vector
609 Laboratories) and cover glass prior to being imaged.

610 Imaging and cell quantification

611 'The Mouse Brain in Stereotaxic Coordinates' provided the framework to label brain
612 sections relative to bregma[84]. A Leica DM6 B epifluorescent microscope was used to image all
613 sections. For eYFP visualization, a YFP filter cube (Excitation: 490-510, Dichroic: 515, Emission:
614 520-550) was used and for tdTomato visualization, a Texas Red Filter Cube (Excitation: BP
615 560/40, Dichroic: LP 585, Emission: BP 630/75) was used. Fos was labeled by Alexa Flour 488.
616 SuM boundaries were defined by -2.6 to -2.95 rostral to Bregma. The medial mammillary nucleus
617 and the mammillary recess of the 3rd ventricle marked the medial and ventral boundaries while
618 fornix marked the lateral, and fasciculus retroflexus the dorsal boundaries. Images were quantified
619 by a trained laboratory member who was blind to the experimental conditions.

620 Forced-Swim Test for cFos examination

621 For stress induction via forced swim (**Figure S4**)[61, 85], mice were individually placed in
622 a cylindrical container (18 cm in diameter) filled with water at 25 +/- 1 °C for 15 min. Prior to stress
623 force swimming, mice were habituated to the arenas for three days prior to the beginning of FST
624 to minimize stress. 90 mins after forced swim, mice were injected with ketamine and xylazine and
625 were intracardially perfused. Control mice were brought to the behavioral testing area but
626 remained in the home cage until perfusion. Water was replaced after every animal. To examine
627 SuM-POA glutamatergic projections, VGlut2-Cre+ littermates were injected with AAV2 retro-Ef1a-
628 DIO-mCherry into the POA.

629 Fiber Photometry

630 For all fiber photometry experiments, the same strategy to selectively label
631 $SuM^{VGLUT2+}$::POA neurons was used. VGLUT2-Flp mice were injected bilaterally in POA with AAV-
632 Retro-EF1a-fDIO-Cre and with AAV-syn-FLEX-GCaMP7s-WPRE in SuM. After two weeks, mice
633 were implanted with fiber-optic cannulas (200µm) in SuM (D/V -4.3-5)[86]. Mice recovered a
634 minimum of one week prior to behavioral testing. Recording of Ca^{2+} dependent and isosbestic
635 signals were obtained using previously described methods with Bonsai software and FP3002
636 (Neurophotometrics)[59, 87]. 470 and 415 nm LEDs were used to record interleaved isosbestic
637 and Ca^{2+} dependent signals following the manufacturer directions.

638 For repeated forced swim experiments (dunk tank), mice were placed on top of a square
639 wire mesh platform inside a custom-made plastic rectangular enclosure (20 cm x 20 cm x 23 cm)
640 filled with water 30 +/- 1 °C. The square wire mesh platform could be raised and lowered without
641 touching the animal. Mice were habituated for 2 days before the test day. Each day, mice were
642 tethered to the fiber optic patch cable and placed on top of the platform for 30mins. On test day,
643 mice were tethered and placed on top of the platform for 30mins (habituation) before the beginning
644 of the 1st trial. After 30mins, for each trial the platform was lowered for 30s and raised after 30s
645 with a rest of 2mins between trials for a total of 10 trials ("dunks"). After 10 trials, an additional
646 2mins were recorded before removing the animal from the enclosure, patted the animals with
647 paper towels, and placed back in its home cage. During testing, mice were tethered to a fiberoptic
648 patch cable that was attached to a counterbalanced arm that prevented downward force on the
649 animal. Water was replaced after each animal. Time mobile was quantified by a trained observer
650 for the ten 30s trials.

651 For foot shock stress testing, mice were individually placed inside a custom-made clear
652 plastic box (15.24 L x 13.34 W x 14 H cm) inside a sound-attenuated cabinet. A speaker was
653 placed 4 cm above the chamber for the delivery of auditory cues (75dB). A constant current
654 aversive stimulator (ENV-414S) delivered foot shocks through a grid floor (0.7mA). Five shocks
655 of 2s were delivered after a 30s tone. Intertrial interval ranged from 90 to 180s. After the session,
656 the animal was removed from the chamber and placed back in its home cage. The chamber and
657 grid were wiped down with 70% ethanol between animals.

658 For open field testing velocity measurements, mice were tethered to a fiberoptic patch
659 cable and placed inside a custom-built square arena (50.8 cm x 50.8 cm x 50.8 cm). Mice were
660 allowed to explore the arena for a 20 min session. Velocity was quantified using scripts in Bonsai
661 2.4. Bedding in the arena was replaced between animals, and the floors and walls of the arena
662 were wiped down with 70% ethanol.

663 Similar to the repeated forced swim experiments, forced swim mice were placed on top of
664 a square wire mesh platform that could be raised and lowered inside a custom-made plastic
665 rectangular enclosure (20 cm x 20 cm x 23 cm) filled with water at 25 +/- 1 °C. The platform was
666 lowered at the beginning of the test for 15 min and raised at the conclusion of the test. During
667 testing, mice were tethered to a fiberoptic patch cable that was attached to a counter balanced
668 arm that prevented downward force on the animal. Water was replaced between animals and the
669 enclosure was wiped down with 70% ethanol and rinsed with water. Time immobile, hindpaw
670 swim, swimming, and climbing were quantified using LabGym (Hu et al., 2022).
671 To measure the activity of $SuM^{VGLUT2+}$::POA neurons in response to a stressor that mice
672 may encounter in their natural habitat[88], a remote-controlled spider was used to simulate an
673 ambush of a potential predator. The remote-controlled spider (17 cm x 16 cm; Amazon) was
674 placed inside a polylactic acid (PLA) enclosure (19 cm x 20 cm x 23 cm) that was then placed
675 inside a custom-built square arena (50.8 cm x 50.8 cm x 50.8 cm). Mice were tethered to a
676 fiberoptic patch cable and placed inside the arena for 10 min. Baseline activity was recorded for
677 5 min before the ambush. After 5 min, the animal was ambushed once it moved in close proximity
678 to the spider's enclosure (Supplemental video 4). Velocity was measured and analyzed using
679 DeepLabCut (Mathis et al., 2019) within Bonsai. The arena and spider's enclosure were wiped
680 down with 70% ethanol between animals.
681 For experiments that examined recruitment of $SuM^{VGLUT2+}$::POA neurons during
682 consummatory behavior, mice were food deprived or given ad lib access to food for 24 hours prior
683 to testing. On test day, mice were placed inside an 18 cm diameter round arena and allowed to
684 habituate for 30 min before they were tethered to the fiberoptic path cable. Once tethered, mice
685 were placed inside the arena for 20 min. Baseline activity was recorded for 5 min before the
686 introduction of the chow pellet and for 15 min after the chow pellet was introduced. Chow pellets
687 were weighed before and after the 20-min trial. The difference is reported as food eaten. The
688 same procedure was followed for control mice with the only difference being that these animals
689 were not food deprived for 24 hours.
690 For fiber photometry data analysis, the interleaved isosbestic and Ca^{2+} dependent signals
691 were recorded at 60 fps (30 fps each). Deinterleaved signals were analyzed using methods as
692 previously reported [87]. Briefly, raw signals were smoothed using a moving average, fitted with
693 an exponential curve using a non-linear least squares function for baseline correction, signals
694 were standardized using the mean value and standard deviation (Z-Score), the standardized
695 isosbestic and Ca2+ signals were scaled a non-negative robust linear regression, and normalized
696 dF/F was calculated. In experiments shown in figures 7A and 8 E-F there was sustained step drop

697 evident in the Ca^{2+} dependent signal reflecting change in population activity because it was not
698 seen in the isosbestic signal. The nature and duration of the change of the signal precluded fitting
699 a curve to the Ca^{2+} dependent signal. In these cases, we show both the Ca^{2+} dependent and
700 isosbestic signals. Z-scores were calculated without baseline correction for both Ca^{2+} dependent
701 and isosbestic signals based on the variability in the baseline state.

702 Real-time place aversion testing

703 For real-time place preference testing with optogenetic photostimulation, we used custom-
704 made, unbiased, balanced two-compartment conditioning apparatus (52.5 x 25.5 x 25.5 cm) as
705 described previously[78, 79, 89]. Mice were tethered to a patch cable that allowed free access to
706 the entire arena for 30 min. Entry into one compartment triggered photostimulation, 1 Hz, 5 Hz,
707 10 Hz, or 20 Hz (473 nm laser, 10 ms pulse width), that persisted while the mouse remained in
708 the light paired side. The side paired with photostimulation was counterbalanced across mice.
709 Ordering was counterbalanced with respect to stimulation frequency and placement. Bedding in
710 the behavior apparatus was replaced between every trial, and the floors and walls of the
711 apparatus were wiped down with 70% ethanol. Time spent in each chamber and total distance
712 traveled for the entire 30-min trial was measured using Ethovision 10 (Noldus Information
713 Technologies). For optogenetic stimulation of VGAT neurons during RTTA, Cre+ littermates were
714 injected either with AAV5-EF1a-DIO-hChR2(H134R)-EYFP or with AAV5-EF1a-DIO-eYFP as
715 control, and stimulation was provided at 10 Hz.

716 Light /Dark choice

717 For light/dark choice, the same arenas as used for real-time preference testing were
718 modified and used as previously described [90]. On the light side, a small sport light was placed
719 overhead, and the walls were covered with white laminated paper. Light levels on this side
720 measure 580-590 lux. For the dark side, an infrared spotlight was placed over head, to allow for
721 video tracking of the mice. The walls were covered with matte black plastic. Light levels in the
722 center of the dark side measure 100-110 lux. Animals were recorded using a USB web cam
723 without an infrared filter. For real-time aversion testing, photostimulation was paired with the dark
724 side of the arena as described above. For anxiety-like behavior testing, stimulation was provided
725 uniformly during the trials. Time spent in each chamber and total distance traveled for the entire
726 30-min trial was measured using Ethovision 10.

727 Observational behavioral assay

728 To observe behaviors evoked by photostimulation of $SuM^{VGLUT2+}$::POA neurons, mice
729 were habituated for at least three days prior to testing to a round (18 cm diameter), clear arena
730 with counterbalanced optical commutators to minimize the impact of the head tether on

731 movement. Testing occurred after habitation, and approximately 2 cm of bedding material was
732 placed in the arena. Behavior was recorded from the side and scored by a blinded observer.
733 Negative reinforcer two nose port operant behavior testing
734 For operant behavior testing, we used Med Associates mouse operant conditioning
735 chamber with dual nose ports and house light as previously described[59]. Briefly, mice were
736 tethered via cantilevered counterweighted optical commutator to a laser light source. A five-day
737 protocol call was used. Day one through four were 10-min trials. Photostimulation was provided
738 at 10 Hz and activation of the active port resulted in a 10-second pause in the photostimulation
739 and activation of the house light inside the arena. On the first four days, each activation of the
740 active port outside of a 10-second pause resulted in a new pause. On day five was a 30-min trial
741 using a progressive ratio protocol the number activation of the active port to generate a pause
742 increased with each activation based on the $number\ of\ activations\ (j) = [5e^{(0.2j)} - 5]$ round to
743 the nearest integer generating the schedule 1, 2, 4, 6, 9, 12, 15, 20, 25, 32, 40, 50….[91]. The
744 trial was limited to 30-mins due to concern for animal welfare due to the head tether and confined
745 space. Photostimulation terminated at the conclusion of the trial.
746 Forced Swim with photostimulation
747 Forced swim trials with optogenetic stimulation were done as a two-day test. On the first
748 day, all mice were subjected to a 15-min forced swim, dried, and returned to the home cage. On
749 the second day, they were tethered and subjected to a 6-min forced swim, divided into three
750 periods, each two mins in length: pre stimulation, stimulation, and post stimulation. 10 Hz
751 photostimulation was provided during the trial. Mice were closely monitored during each trial of
752 swimming. Trials were recorded and scored by a blinded observer for time spent immobile on the
753 second day of the test. For forced swim trials with optogenetic stimulation of VGAT neurons, Cre+
754 littermates were injected either with AAV5-EF1a-DIO-hChR2(H134R)-EYFP or with AAV5-EF1a-
755 DIO-eYFP as control.
756 Feeding after food deprivation
757 For tests involving brief access to food after deprivation, the same 18 cm diameter round
758 arenas with counterbalanced optical commutators were used. Mice were habituated to the arenas
759 for a minimum of three days prior to testing. Mice were food deprived by removal of food from the
760 home cage 24 hours prior to testing. Mice were placed in the arena and allowed to habituate prior
761 to introduction of a chow pellet. The 20-min trial with the foot pellet was recorded and scored by
762 a blinded observer. Chow pellets were weighed before and after the 20-min trial. The difference
763 is reported as food eaten.
764 Open Field Test

765 For Open Field testing, we used a purpose-built 20 in square behavior arena. Mice were
766 tethered to a patch cable and placed into the behavioral arena. The laser frequency was set to 10
767 Hz and was left on for 20 mins. Distance moved for the 20-min trial was quantified using
768 Ethovision 10. Bedding in the arena was replaced between every trial, and the floors and walls of
769 the arena were wiped down with 70% ethanol. Similarly, for optogenetic stimulation of VGAT
770 neurons, Cre+ littermates were injected either with AAV5-EF1a-DIO-hChR2(H134R)-EYFP or
771 with AAV5-EF1a-DIO-eYFP as control.

772 Statistical analyses

773 Statistical analyses were conducted using GraphPad Prism software. Data are shown as
774 mean ±SEM, except for Z-scores which are shown as ± 95% confidence interval, as noted in text.
775 Values for individual p values are given in the text and figure legends. Significance was held at α
776 less than 0.05. Unless noted in the test, nonparametric Mann-Whitney tests were used for
777 statistical comparisons. In cases of multiple comparisons, Holm-Šídák method was used to
778 correct for multiple comparisons. Paired testing was used with comparing within cohorts with
779 repeated measurements and unpaired between cohorts. All “n” values represent the number of
780 animals in a particular group for an experiment. For fiber photometry statistical analysis, the mean
781 signal of the baseline and stimulus windows was used, and comparisons were made using the
782 Wilcoxon ranked-sum test, with α=0.95. To analyze the change in the Ca^{2+} dependent signal, a t-
783 confidence interval method was used, in which 95%, 99%, and 99.9% confidence intervals were
784 calculated for windows preceding and subsequently following the described point of interest.
785 Differences were considered significant if the null hypothesis (zero) was not included in the CI.
786 Because exact p values are not calculated using this method, the highest confidence level at
787 which the difference is significant (95%, 99%, or 99.9% CI) is reported instead.

Citations

1. LeDoux, J. and N.D. Daw, *Surviving threats: neural circuit and computational implications of a new taxonomy of defensive behaviour.* Nat Rev Neurosci, 2018. **19**(5): p. 269-282.
2. LeDoux, J.E., *Coming to terms with fear.* Proc Natl Acad Sci U S A, 2014. **111**(8): p. 2871-8.
3. Mobbs, D., et al., *The ecology of human fear: survival optimization and the nervous system.* Front Neurosci, 2015. **9**: p. 55.
4. Shin, L.M. and I. Liberzon, *The neurocircuitry of fear, stress, and anxiety disorders.* Neuropsychopharmacology, 2010. **35**(1): p. 169-91.
5. Ressler, K.J. and H.S. Mayberg, *Targeting abnormal neural circuits in mood and anxiety disorders: from the laboratory to the clinic.* Nat Neurosci, 2007. **10**(9): p. 1116-24.
6. Kessler, R.C., et al., *Lifetime prevalence and age-of-onset distributions of mental disorders in the World Health Organization's World Mental Health Survey Initiative.* World Psychiatry, 2007. **6**(3): p. 168-76.
7. Southwick, S.M., M. Vythilingam, and D.S.J.A.R.C.P. Charney, *The psychobiology of depression and resilience to stress: implications for prevention and treatment.* 2005. **1**: p. 255-291.
8. Penzo, M.A., et al., *The paraventricular thalamus controls a central amygdala fear circuit.* Nature, 2015. **519**(7544): p. 455-9.
9. Ma, J., et al., *Divergent projections of the paraventricular nucleus of the thalamus mediate the selection of passive and active defensive behaviors.* Nat Neurosci, 2021. **24**(10): p. 1429-1440.
10. Ledoux, J.E. and J.M. Gorman, *A call to action: Overcoming anxiety through active coping.* American Journal of Psychiatry, 2001. **158**(12): p. 1953-1955.
11. Steimer, T., *Animal models of anxiety disorders in rats and mice: some conceptual issues.* Dialogues Clin Neurosci, 2011. **13**(4): p. 495-506.
12. Gross, C.T. and N.S. Canteras, *The many paths to fear.* Nat Rev Neurosci, 2012. **13**(9): p. 651-8.
13. Amorapanth, P., J.E. LeDoux, and K. Nader, *Different lateral amygdala outputs mediate reactions and actions elicited by a fear-arousing stimulus.* Nature Neuroscience, 2000. **3**(1): p. 74-79.
14. Canteras, N.S., et al., *Severe reduction of rat defensive behavior to a predator by discrete hypothalamic chemical lesions.* Brain Res Bull, 1997. **44**(3): p. 297-305.
15. Pan, W.X. and N. McNaughton, *The supramammillary area: its organization, functions and relationship to the hippocampus.* Prog Neurobiol, 2004. **74**(3): p. 127-66.
16. Vertes, R.P. and J.T. McKenna, *Collateral projections from the supramammillary nucleus to the medial septum and hippocampus.* Synapse, 2000. **38**(3): p. 281-293.
17. Vertes, R.P., *Pha-L Analysis of Projections from the Supramammillary Nucleus in the Rat.* Journal of Comparative Neurology, 1992. **326**(4): p. 595-622.
18. Kiss, J., et al., *Possible glutamatergic/aspartatergic projections to the supramammillary nucleus and their origins in the rat studied by selective [(3)H]D-aspartate labelling and immunocytochemistry.* Neuroscience, 2002. **111**(3): p. 671-91.
19. Kesner, A.J., et al., *Supramammillary neurons projecting to the septum regulate dopamine and motivation for environmental interaction in mice.* Nat Commun, 2021. **12**(1): p. 2811.
20. Li, Y., et al., *Supramammillary nucleus synchronizes with dentate gyrus to regulate spatial memory retrieval through glutamate release.* Elife, 2020. **9**.
21. Billwiller, F., et al., *GABA-glutamate supramammillary neurons control theta and gamma oscillations in the dentate gyrus during paradoxical (REM) sleep.* Brain Struct Funct, 2020. **225**(9): p. 2643-2668.
22. Ito, H.T., E.I. Moser, and M.B. Moser, *Supramammillary Nucleus Modulates Spike-Time Coordination in the Prefrontal-Thalamo-Hippocampal Circuit during Navigation.* Neuron, 2018. **99**(3): p. 576-587 e5.

23. Pedersen, N.P., et al., *Supramammillary glutamate neurons are a key node of the arousal system.* Nature Communications, 2017. **8**.
24. Leranth, C. and J. Kiss, *A population of supramammillary area calretinin neurons terminating on medial septal area cholinergic and lateral septal area calbindin-containing cells are aspartate/glutamatergic.* J Neurosci, 1996. **16**(23): p. 7699-710.
25. Swanson, L.J.B.r.b., *The projections of the ventral tegmental area and adjacent regions: a combined fluorescent retrograde tracer and immunofluorescence study in the rat.* 1982. **9**(1-6): p. 321-353.
26. Kocsis, K., et al., *Location of putative glutamatergic neurons projecting to the medial preoptic area of the rat hypothalamus.* Brain Res Bull, 2003. **61**(4): p. 459-68.
27. Pan, W.-X. and N.J.P.i.n. McNaughton, *The supramammillary area: its organization, functions and relationship to the hippocampus.* 2004. **74**(3): p. 127-166.
28. Soussi, R., et al., *Heterogeneity of the supramammillary–hippocampal pathways: Evidence for a unique GABAergic neurotransmitter phenotype and regional differences.* 2010. **32**(5): p. 771-785.
29. Haglund, L., L.W. Swanson, and C. Kohler, *The Projection of the Supramammillary Nucleus to the Hippocampal-Formation - an Immunohistochemical and Anterograde Transport Study with the Lectin Pha-L in the Rat.* Journal of Comparative Neurology, 1984. **229**(2): p. 171-185.
30. Hayakawa, T., H. Ito, and K. Zyo, *Neuroanatomical Study of Afferent-Projections to the Supramammillary Nucleus of the Rat.* Anatomy and Embryology, 1993. **188**(2): p. 139-148.
31. Hashimotodani, Y., et al., *Supramammillary Nucleus Afferents to the Dentate Gyrus Co-release Glutamate and GABA and Potentiate Granule Cell Output.* Cell Rep, 2018. **25**(10): p. 2704-2715 e4.
32. Park, Y.G., et al., *Protection of tissue physicochemical properties using polyfunctional crosslinkers.* Nat Biotechnol, 2018.
33. Madisen, L., et al., *A robust and high-throughput Cre reporting and characterization system for the whole mouse brain.* Nat Neurosci, 2010. **13**(1): p. 133-40.
34. Li, Y., et al., *Supramammillary nucleus synchronizes with dentate gyrus to regulate spatial memory retrieval through glutamate release.* 2020. **9**: p. e53129.
35. Wyss, J., et al., *Evidence for an input to the molecular layer and the stratum granulosum of the dentate gyrus from the supramammillary region of the hypothalamus.* 1979. **156**(2): p. 165-176.
36. Hashimotodani, Y., et al., *Supramammillary nucleus afferents to the dentate gyrus co-release glutamate and GABA and potentiate granule cell output.* 2018. **25**(10): p. 2704-2715. e4.
37. Nakanishi, K., H. Saito, and K.J.E.J.o.N. Abe, *The supramammillary nucleus contributes to associative EPSP-spike potentiation in the rat dentate gyrus in vivo.* 2001. **13**(4): p. 793-800.
38. Maglóczky, Z., L. Acsády, and T.F.J.H. Freund, *Principal cells are the postsynaptic targets of supramammillary afferents in the hippocampus of the rat.* 1994. **4**(3): p. 322-334.
39. Day, H.E., C.V. Masini, and S. Campeau, *The pattern of brain c-fos mRNA induced by a component of fox odor, 2,5-dihydro-2,4,5-trimethylthiazoline (TMT), in rats, suggests both systemic and processive stress characteristics.* Brain Res, 2004. **1025**(1-2): p. 139-51.
40. Santin, L.J., et al., *c-Fos expression in supramammillary and medial mammillary nuclei following spatial reference and working memory tasks.* Physiol Behav, 2003. **78**(4-5): p. 733-9.
41. Azevedo, E.P., et al., *A limbic circuit selectively links active escape to food suppression.* eLife, 2020. **9**: p. e58894.
42. Farrell, J.S., et al., *Supramammillary regulation of locomotion and hippocampal activity.* Science, 2021. **374**(6574): p. 1492-1496.
43. De Boer, S.F. and J.M. Koolhaas, *Defensive burying in rodents: ethology, neurobiology and psychopharmacology.* Eur J Pharmacol, 2003. **463**(1-3): p. 145-61.

44. Castro, D.C., R.A. Terry, and K.C. Berridge, *Orexin in Rostral Hotspot of Nucleus Accumbens Enhances Sucrose 'Liking' and Intake but Scopolamine in Caudal Shell Shifts 'Liking' Toward 'Disgust' and 'Fear'.* Neuropsychopharmacology, 2016. **41**(8): p. 2101-11.
45. Reynolds, S.M. and K.C. Berridge, *Fear and feeding in the nucleus accumbens shell: rostrocaudal segregation of GABA-elicited defensive behavior versus eating behavior.* J Neurosci, 2001. **21**(9): p. 3261-70.
46. Richard, J.M. and K.C. Berridge, *Nucleus accumbens dopamine/glutamate interaction switches modes to generate desire versus dread: D(1) alone for appetitive eating but D(1) and D(2) together for fear.* J Neurosci, 2011. **31**(36): p. 12866-79.
47. Kalueff, A.V. and P.J.B.R.P. Tuohimaa, *Grooming analysis algorithm for neurobehavioural stress research.* 2004. **13**(3): p. 151-158.
48. van Erp, A.M., et al., *Effect of environmental stressors on time course, variability and form of self-grooming in the rat: handling, social contact, defeat, novelty, restraint and fur moistening.* Behav Brain Res, 1994. **65**(1): p. 47-55.
49. Kravitz, A.V., L.D. Tye, and A.C. Kreitzer, *Distinct roles for direct and indirect pathway striatal neurons in reinforcement.* Nat Neurosci, 2012. **15**(6): p. 816-8.
50. McCall, J.G., et al., *CRH Engagement of the Locus Coeruleus Noradrenergic System Mediates Stress-Induced Anxiety.* Neuron, 2015. **87**(3): p. 605-20.
51. Felix-Ortiz, A.C., et al., *BLA to vHPC inputs modulate anxiety-related behaviors.* Neuron, 2013. **79**(4): p. 658-64.
52. Jakovcevski, M., M. Schachner, and F. Morellini, *Susceptibility to the long-term anxiogenic effects of an acute stressor is mediated by the activation of the glucocorticoid receptors.* Neuropharmacology, 2011. **61**(8): p. 1297-305.
53. Bailey, K.R. and J.N. Crawley, *Anxiety-Related Behaviors in Mice*, in *Methods of Behavior Analysis in Neuroscience*, nd and J.J. Buccafusco, Editors. 2009: Boca Raton (FL).
54. Heredia, L., et al., *Assessing anxiety in C57BL/6J mice: a pharmacological characterization of the open-field and light/dark tests.* 2014. **69**(2): p. 108-114.
55. Prut, L. and C.J.E.j.o.p. Belzung, *The open field as a paradigm to measure the effects of drugs on anxiety-like behaviors: a review.* 2003. **463**(1-3): p. 3-33.
56. Chaouloff, F., M. Durand, and P.J.B.b.r. Mormède, *Anxiety-and activity-related effects of diazepam and chlordiazepoxide in the rat light/dark and dark/light tests.* 1997. **85**(1): p. 27-35.
57. Mobbs, D., et al., *The ecology of human fear: survival optimization and the nervous system.* 2015. **9**: p. 55.
58. Fadok, J.P., et al., *A competitive inhibitory circuit for selection of active and passive fear responses.* Nature, 2017. **542**(7639): p. 96-100.
59. Parker, K.E., et al., *A Paranigral VTA Nociceptin Circuit that Constrains Motivation for Reward.* Cell, 2019. **178**(3): p. 653-671 e19.
60. Costa, A.P., et al., *A proposal for refining the forced swim test in Swiss mice.* Prog Neuropsychopharmacol Biol Psychiatry, 2013. **45**: p. 150-5.
61. Commons, K.G., et al., *The Rodent Forced Swim Test Measures Stress-Coping Strategy, Not Depression-like Behavior.* ACS Chem Neurosci, 2017. **8**(5): p. 955-960.
62. Hu, Y., et al., *LabGym: quantification of user-defined animal behaviors using learning-based holistic assessment.* 2022: p. 2022.02.17.480911.
63. Seo, C., et al., *Intense threat switches dorsal raphe serotonin neurons to a paradoxical operational mode.* 2019. **363**(6426): p. 538-542.
64. Chen, S., et al., *A hypothalamic novelty signal modulates hippocampal memory.* Nature, 2020. **586**(7828): p. 270-274.

65. Andalman, A.S., et al., *Neuronal Dynamics Regulating Brain and Behavioral State Transitions.* Cell, 2019. **177**(4): p. 970-985 e20.
66. Berton, O., et al., *Induction of deltaFosB in the periaqueductal gray by stress promotes active coping responses.* Neuron, 2007. **55**(2): p. 289-300.
67. Tovote, P., et al., *Midbrain circuits for defensive behaviour.* Nature, 2016. **534**(7606): p. 206-12.
68. Keay, K.A. and R. Bandler, *Parallel circuits mediating distinct emotional coping reactions to different types of stress.* Neurosci Biobehav Rev, 2001. **25**(7-8): p. 669-78.
69. Lee, A., et al., *The habenula prevents helpless behavior in larval zebrafish.* Curr Biol, 2010. **20**(24): p. 2211-6.
70. Li, B., et al., *Synaptic potentiation onto habenula neurons in the learned helplessness model of depression.* Nature, 2011. **470**(7335): p. 535-9.
71. Lazaridis, I., et al., *A hypothalamus-habenula circuit controls aversion.* 2019. **24**(9): p. 1351-1368.
72. Mondoloni, S., M. Mameli, and M.J.T.P. Congiu, *Reward and aversion encoding in the lateral habenula for innate and learned behaviours.* 2022. **12**(1): p. 3.
73. Keay, K.A. and R. Bandler, *Parallel circuits mediating distinct emotional coping reactions to different types of stress.* Neuroscience and Biobehavioral Reviews, 2001. **25**(7-8): p. 669-678.
74. Cryan, J.F., R.J. Valentino, and I. Lucki, *Assessing substrates underlying the behavioral effects of antidepressants using the modified rat forced swimming test.* Neurosci Biobehav Rev, 2005. **29**(4-5): p. 547-69.
75. Knoll, A.T. and W.A.J.B.r. Carlezon Jr, *Dynorphin, stress, and depression.* 2010. **1314**: p. 56-73.
76. Ebner, K. and N.J.C.O.i.B.S. Singewald, *Individual differences in stress susceptibility and stress inhibitory mechanisms.* 2017. **14**: p. 54-64.
77. Vong, L., et al., *Leptin action on GABAergic neurons prevents obesity and reduces inhibitory tone to POMC neurons.* Neuron, 2011. **71**(1): p. 142-54.
78. Norris, A.J., et al., *Parabrachial opioidergic projections to preoptic hypothalamus mediate behavioral and physiological thermal defenses.* Elife, 2021. **10**.
79. McCall, J.G., et al., *CRH Engagement of the Locus Coeruleus Noradrenergic System Mediates Stress-Induced Anxiety.* Neuron, 2015. **87**(3): p. 605-620.
80. Sparta, D.R., et al., *Construction of implantable optical fibers for long-term optogenetic manipulation of neural circuits.* Nat Protoc, 2011. **7**(1): p. 12-23.
81. Fenno, L.E., et al., *Targeting cells with single vectors using multiple-feature Boolean logic.* Nat Methods, 2014. **11**(7): p. 763-72.
82. Back, S., et al., *Neuron-Specific Genome Modification in the Adult Rat Brain Using CRISPR-Cas9 Transgenic Rats.* Neuron, 2019. **102**(1): p. 105-119 e8.
83. Lee, J.H., et al., *Global and local fMRI signals driven by neurons defined optogenetically by type and wiring.* Nature, 2010. **465**(7299): p. 788-92.
84. Paxinos, G. and K.B. Franklin, *Paxinos and Franklin's the mouse brain in stereotaxic coordinates*. 2019: Academic press.
85. Porsolt, R.D., et al., *Immobility induced by forced swimming in rats: effects of agents which modify central catecholamine and serotonin activity.* Eur J Pharmacol, 1979. **57**(2-3): p. 201-10.
86. Dana, H., et al., *High-performance calcium sensors for imaging activity in neuronal populations and microcompartments.* Nat Methods, 2019. **16**(7): p. 649-657.
87. Martianova, E., S. Aronson, and C.D. Proulx, *Multi-Fiber Photometry to Record Neural Activity in Freely-Moving Animals.* J Vis Exp, 2019(152).
88. Nyffeler, M. and R.S. Vetter, *Black widow spiders, Latrodectus spp. (Araneae: Theridiidae), and other spiders feeding on mammals.* The Journal of Arachnology, 2018. **46**(3): p. 541-548.

975 89. Stamatakis, A.M. and G.D. Stuber, *Activation of lateral habenula inputs to the ventral midbrain*
976 *promotes behavioral avoidance.* Nat Neurosci, 2012. **15**(8): p. 1105-7.
977 90. Luskin, A.T., et al., *Extended amygdala-parabrachial circuits alter threat assessment and regulate*
978 *feeding.* Sci Adv, 2021. **7**(9).
979 91. Richardson, N.R. and D.C. Roberts, *Progressive ratio schedules in drug self-administration studies*
980 *in rats: a method to evaluate reinforcing efficacy.* J Neurosci Methods, 1996. **66**(1): p. 1-11.

Figure 1

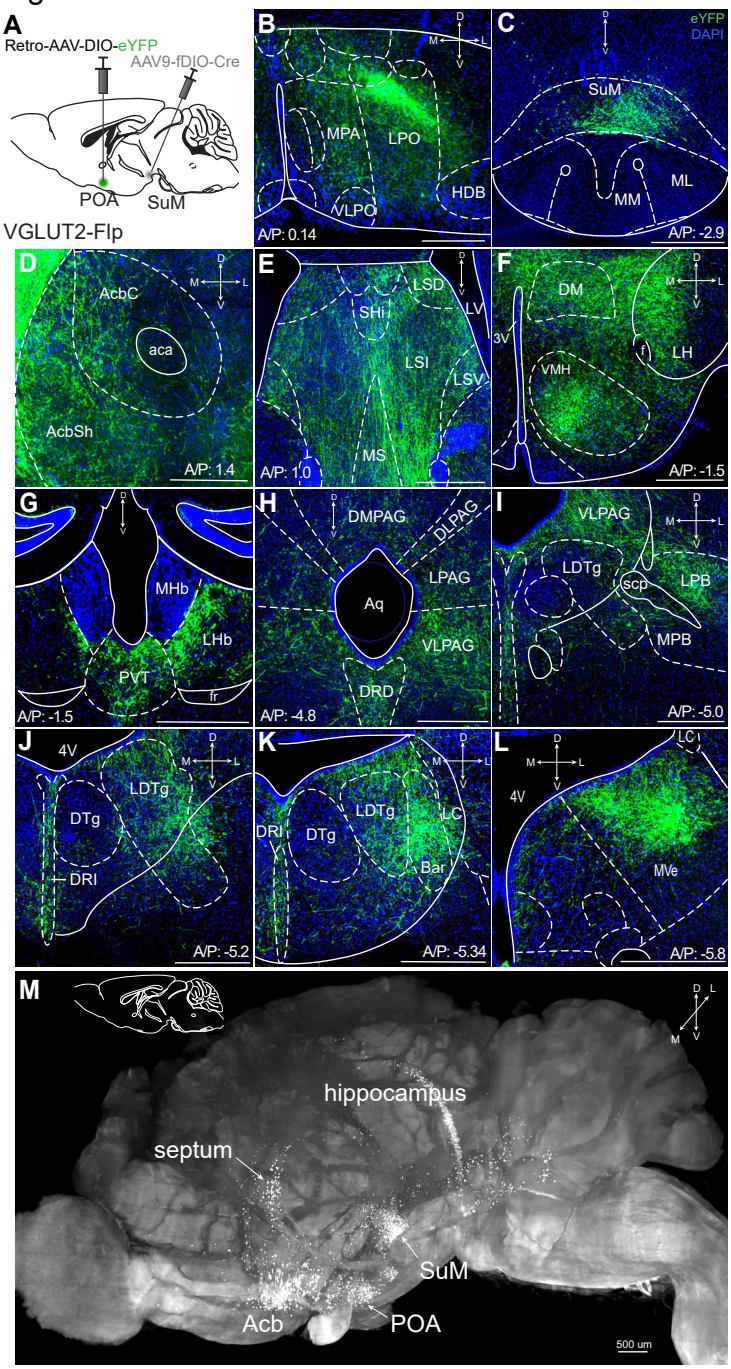

Figure 1. SuM$^{VGLUT2+}$::POA arborize widely in the brain. (A) Schematic of injections of Retro-AAV-DIO-eYFP into the POA and AAV-fDIO-Cre into the SuM of VGLUT2-Flp mice to label only VGLUT+ SuM neurons that project to the POA. (**B**) Projections of VGLUT2+ SuM neurons labeled with eYFP seen in the POA. (**C**) Cell bodies labeled with eYFP in the SuM. (**D-L**) Arborizing processes from the SuM$^{VGLUT2+}$::POA neurons are seen in multiple brain regions including the (**D**) AcbSh and AcbC; (**E**) lateral septum; (**F**) multiple hypothalamic areas; (**G**) lHb and PVT; (**H**) the PAG and the DRD; (**I**) VLPAG and LPB; (**J**) DRI and LDTg; (**K**) and DRI, and MVePC. (**M**) Light sheet microscopy image of a cleared mouse brain hemisphere, viewed from medial to lateral, showing eYFP labeled neurons in SuM$^{VGLUT2+}$::POA with cell bodies in SuM and processes in areas corresponding to septum, hippocampus, Acb, and POA. (500 µm scale bars).

Abbreviations- *MPA*- medial preotic, *VLPO*- ventral lateral preoptic, *LPO*- lateral preotic, *HDB*- nucleus of the horizontal limb of the diagonal band *AcbSh*- Accumbens shell, *AcbC*- Accumbens core, *Shi*- septohippocampal nucleus, *LSI*- lateral septal nucleus, intermediate part, *LSV*- lateral septal nucleus, ventral part, *LV*- lateral ventricle, *MS*- medial septal nucleus, *lHb*- lateral habenula, m*Hb*- medial habenula, *PVT*- paraventricular thalamus, *DM*- dorsomedial hypothalamic nucleus, *LH*- lateral hypothalamic area, *VMH*-

Figure 2

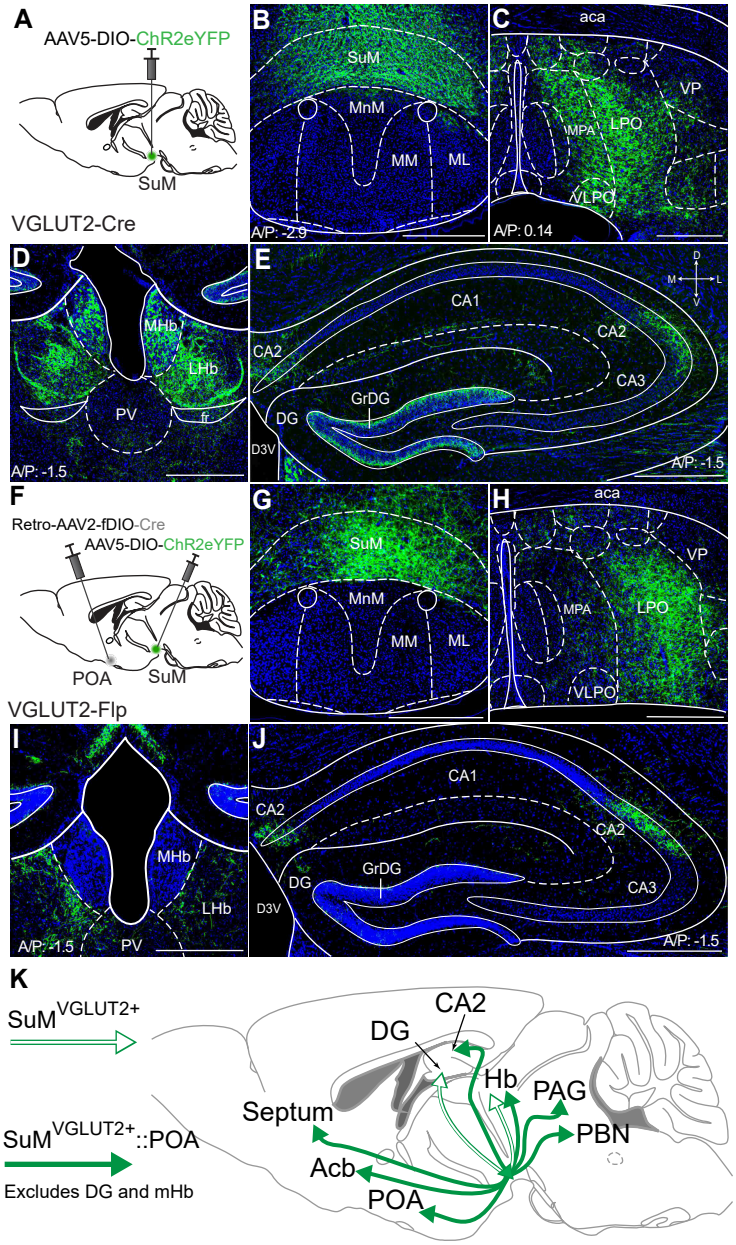

Figure 2. SuM$^{VGLUT2+}$::POA neurons project to a subset of brain regions compared to all SuM$^{VGLUT2+}$ neurons. (**A**) Schematic of injections in VGLUT2-Cre mice of AAV-DIO-ChR2eYFP into SuM. (**B**) eYFP (green) labeled neurons present in SuM and (**C**) processes were observed in the POA. (**D**) Processes from SuM VGLUT2+ neurons were also present in mHb, lHb, and PVT. (**E**) In hippocampus, processes were observed in DG and CA2. (**F**) Schematic of injections in VGLUT2-Flp mice of Retro-AAV-fDIO-Cre and AAV-DIO-ChR2eYFP into SuM. (**G-H**) Cells in SuM and processes in POA were labeled by ChR2eYFP. (**I**) Labeled processes in lHb were evident but none seen in mHb. (**J**) In hippocampus, labeled processes were present in CA2 but not observed in DG. (500 µm scale bars) (**K**) Schematic summary showing the projection to DG and mHb present in the total SuM VGLUT2+ population (outlined arrows) but absent in the SuM$^{VGLUT2+}$::POA population (filled arrows).

Figure 3

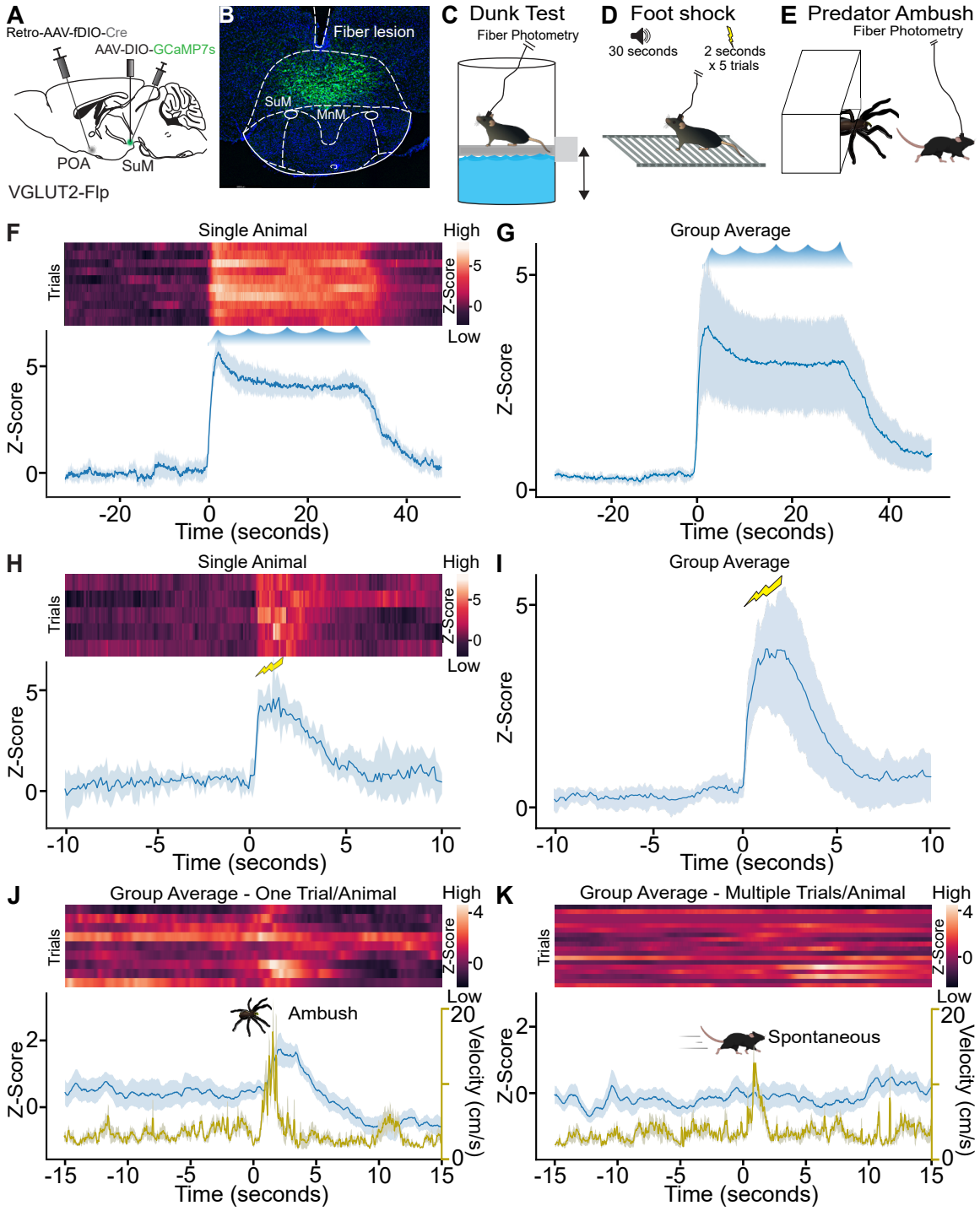
A
Retro-AAV-fDIO-Cre
AAV-DIO-GCaMP7s
POA
SuM
VGLUT2-Flp
B
Fiber lesion
SuM
MnM
C Dunk Test
Fiber Photometry
D Foot shock
30 seconds
2 seconds
x 5 trials
E Predator Ambush
Fiber Photometry
F
Single Animal
High
Low
Trials
Z-Score
Time (seconds)
G
Group Average
H
Single Animal
I
Group Average
J
Group Average - One Trial/Animal
Ambush
Velocity (cm/s)
K
Group Average - Multiple Trials/Animal
Spontaneous

Figure 3. Acute stressors recruit SuM$^{VGLUT2+}$::POA neurons. (**A**) Schematic of VGLUT2-Flp mice injected with AAV-DIO-GCaMP7s in SuM and Retro-AAV-fDIO-Cre in the POA with a (**B**) fiber placed over SuM for fiber photometry recordings from SuM$^{VGLUT2+}$::POA neurons. (**C**) While mice were connected for fiber photometry, they were subjected to ten 30-second trials of forced swimming, (**D**) to a 2-second foot shock following a 30-second tone for five trials, or (**E**) to ambush by a mock predator via remote-controlled spider. (**F**) Heat map and mean ± 95% CI Z-score for recordings obtained from a single animal during the repeated forced swim showing increase Ca^{2+} signal during the swim session. (**G**) The mean ±95% CI Z-score of 10 trials for all animals (n=8) in the dunk assay. (**H**) Heat map and mean ± 95% CI Z-score for recordings from a single animal during the five shock trials showing increase Ca^{2+} signal. (**I)** Mean ± 95% CI Z-score for recordings of five trials for all animals (n=6) in the foot shock assay. (**J**) Heat map, mean ± 95% CI Z-score (blue), mean ± 95% CI velocity (gold), for recordings obtained from animals (n=9) during the ambush showing a significant increase (***99.9% CI) in Ca^{2+} signal as the animals flee from the remote-controlled spider with the mean ±95% confidence interval Z- score of 1 trial (ambush) for all 9 animals. (**K**) Heat map, mean (± 95% CI) Z-score (blue), mean (± 95% CI) velocity (gold), for the same mice but ambush in the predator assay. Time frame gated for spontaneous locomotion. Ca^{2+} signal does not increase significantly during spontaneous locomotion. Mean peak velocity was not significantly different. For Ca^{2+} signal differences: *=95% CI, **=99% CI, ***=99.9% CI, ns=not significant.

Figure 4

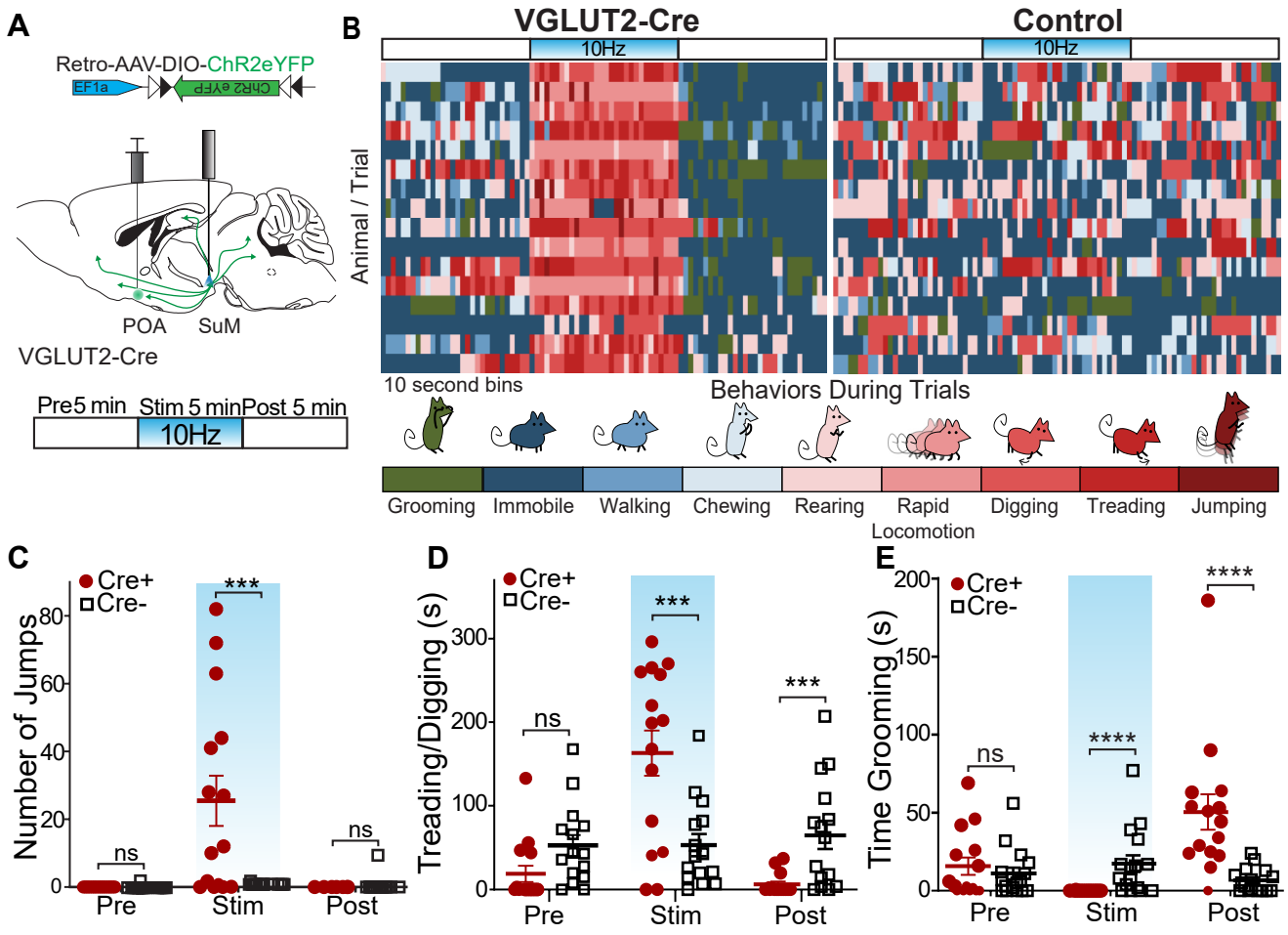

Figure 4. Photostimulation of SuM$^{VGLUT2+}$::POA neurons evokes active coping behaviors. (**A**) Illustration of injections and fiber implant in VGLUT2+ Cre mice and schematic of photostimulation paradigm of 5 min pre, 5 min stimulation, and 5 min post. Behaviors were evaluated during each epoch. (**B**) For Cre+ (n=16) and Cre- (n=16) mice, the behavior in 10s bins was scored based on the predominant behavior displayed during each 10s period for the 15-minute trial into grooming, stationary, walking, chewing, rearing, rapid locomotion, digging (moving bedding towards the tail), treading (move beading forward), and jumping. The graphic shows a by-animal scoring of the 15-minute trial color-coded for each of the behavior categories. (**C**) During the stimulation period, Cre+ (n=15) mice show significantly (*p=0.012) greater jumps than Cre- (n=16) mice, and jumping behaviors were not significantly different during pre and post stim periods. (**D**) Behavior was also scored for time spent moving beading (digging or treading). Cre+ mice showed significantly (**p=0.004) greater time engaging in digging/treading behaviors during the stimulation period, and significantly (*p=0.014) less time during the post-stimulation period compared to Cre- mice. (**E**) Behavior was also scored for time spent engaging in grooming behaviors, and Cre+ mice spent significantly (*p=0.016) less time grooming during the stimulation period and significantly (**p=0.005) more time grooming during the post stimulation period compared to Cre- mice. All data plotted as mean ±SEM.

Figure 5

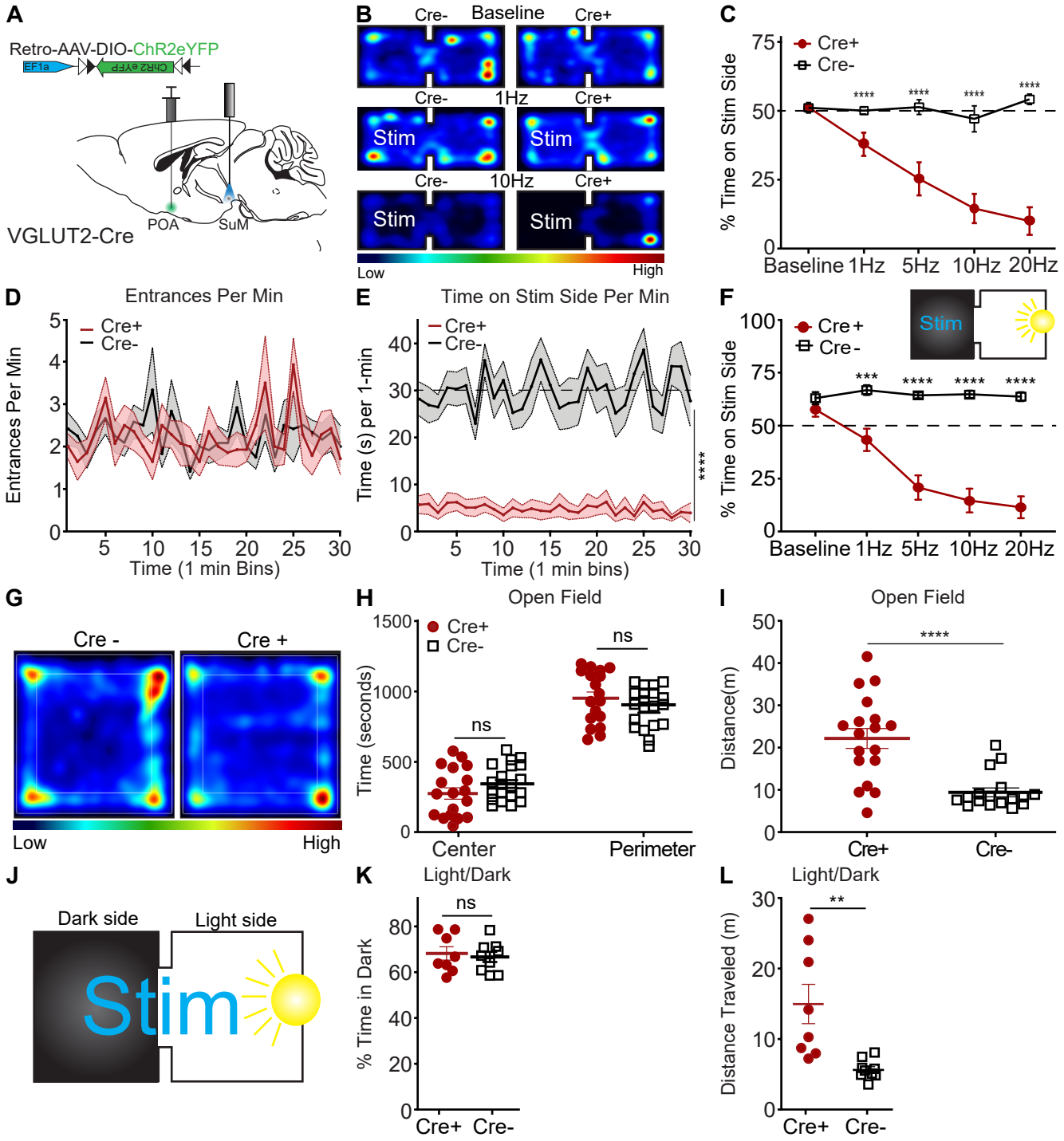
A
Retro-AAV-DIO-ChR2eYFP
EF1a
ChR2 eYFP
POA
SuM
VGLUT2-Cre
B
Cre-
Baseline
Cre+
1Hz
Stim
10Hz
Low
High
C
Cre+
Cre-
% Time on Stim Side
Baseline 1Hz 5Hz 10Hz 20Hz
D
Entrances Per Min
Entrances Per Min
Time (1 min Bins)
E
Time on Stim Side Per Min
Time (s) per 1-min
Time (1 min bins)
F
Stim
% Time on Stim Side
G
Cre -
Cre +
Low
High
H
Open Field
Time (seconds)
ns
Center
Perimeter
I
Open Field
Distance(m)
Cre+
Cre-
J
Dark side
Light side
Stim
K
Light/Dark
% Time in Dark
L
Light/Dark
Distance Traveled (m)

Figure 5. Activation of SuM$^{VGLUT2+}$::POA neurons drives aversion but does not promote anxiety-like behavior (**A**) Schematic of injection of Retro-AAV-ChR2eYFP into the POA and placement of a midline optic fiber over SuM. (**B**) Representative heat maps for Cre+ and Cre- mice at baseline (no stim) and 10 Hz photostimulation in two-sided arena with photostimulation associated with one side. (**C**) Quantification of time spent on stimulation side for Cre+ (n =19) and control Cre- (n=21) mice showing frequency dependent increase in avoidance of the stimulation side of the area (***p<0.001, ****p<0.0001). (**D**) Mean ±SEM entrances per min (in 1-min bins) to the during 10 Hz stimulation trials were not significantly (p=0.87) different between Cre+ (n=14) and Cre- (n=13) mice. (**E**) Mean time spent on the stimulation side for Cre- and Cre+ in 1-minute bins during 10 Hz stimulation trials was significantly (p<0.0001) lower in Cre+ mice. (**F**) (Inset) Diagram of light/dark arena with photostimulation provided on the dark side of the arena and quantification of time spent on dark (stimulation) side, demonstrating that Cre- (n=12) animals show a baseline preference for the dark side of arena that is overcome by photostimulation with Cre+ (n=13) mice spending significantly (**p=0.002, ***p<0.001, ****p<0.0001) less time on the stimulation side. (**G**) Representative heat map of Cre- and Cre+ during 10 Hz photostimulation in open field test. (**H**) In the open field test, time spent in center and perimeter were not significantly different (p=0.19) between Cre+ (n=18) and Cre- (n=17) during 10 Hz photostimulation. (**I**) Distance traveled during open field testing was significantly (p<0.001) increased in Cre+ compared to Cre- mice. (**J**) Schematic of real time light/dark choice testing with stimulation provided at 10 Hz throughout the arena. (**K**) Both Cre+ (n=8) and Cre- (n=9) mice showed a preference for the dark portion of the arena but were not significantly (p=0.9) different. (**L**) The total distance traveled by Cre+ mice were significantly (p=0.003) greater than Cre- mice. All data plotted as mean ±SEM.

Figure 6

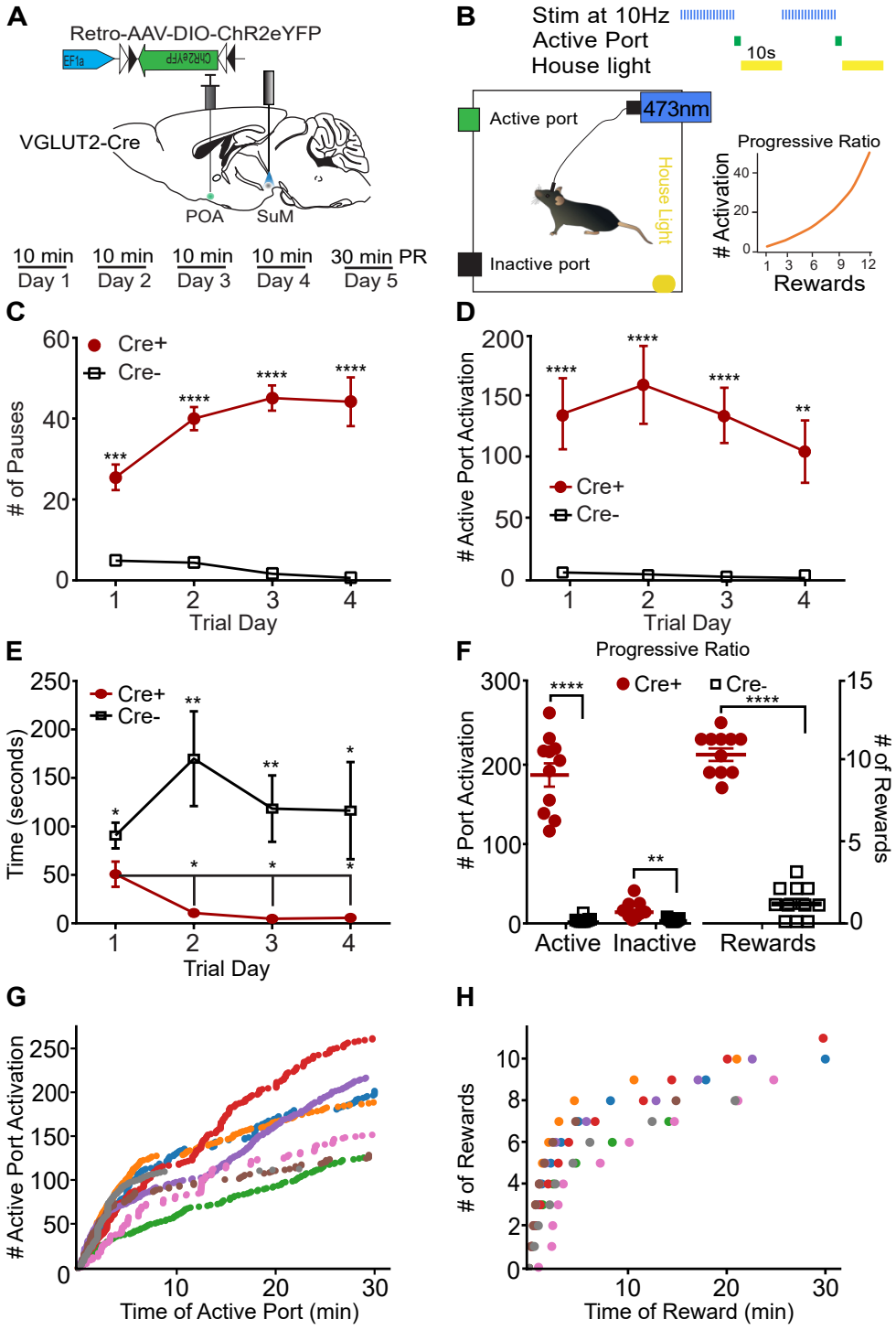
A
Retro-AAV-DIO-ChR2eYFP
EF1a
ChR2eYFP
VGLUT2-Cre
POA
SuM
10 min Day 1
10 min Day 2
10 min Day 3
10 min Day 4
30 min PR Day 5
B
Stim at 10Hz
Active Port
House light
10s
Active port
473nm
House Light
Inactive port
Progressive Ratio
Activation
Rewards
C
Cre+
Cre-
# of Pauses
Trial Day
D
Active Port Activation
Trial Day
E
Time (seconds)
Trial Day
F
Progressive Ratio
Port Activation
of Rewards
Active
Inactive
Rewards
G
Active Port Activation
Time of Active Port (min)
H
# of Rewards
Time of Reward (min)

Figure 6. SuM$^{VGLUT2+}$::POA neurons can drive instrumental action-outcome operant behavior (**A**) Schematic of injection and implant in VGLUT2+ Cre mice and paradigm of testing in 10-minute trials with four days before a progressive ratio (PR) trial on day five. (**B**) Illustration of the testing paradigm and set up. 10 Hz photostimulation was applied during the trials. Activation of the active port triggered the house light and paused stimulation for 10 seconds. Also shown is the progressive ratio used with number of required port activations per reward on vertical axis and reward number on the horizontal. (**C**) Cre+ mice (n=11) activated the active port triggering significantly (****p<0.0001) more pauses in stimulation than Cre- mice (n=11) mice on all four days of testing. (**D**) Cre+ mice activated the port significantly (****p<0.0001, ***p<0.001) more than the Cre- mice on all four trials. (**E**) The time to first activation of the active port was significantly (*p=0.046) different during the first trial, and Cre+ mice activated the active port significantly (**p<0.01, **p<0.01, **p=0.034) faster on subsequent trials. (**F**) On the fifth day after four 10-minute trials, mice were tested for 30 minutes using a progressive ratio. Cre+ performed significantly (****p<0.001) more active port activations than Cre- mice and activated the inactive port significantly more (**p=0.001) times. Cre+ mice also triggered significantly (****p<0.001) more pauses in photostimulation than Cre- mice. (**G**) Individual data for a representative (n=7) cohort of Cre+ mice showing cumulative active port activations as a function of time during the progressive ratio test show on-going engagement of the active port throughout the 30-minute trial. (**H**) The cumulative pauses in photostimulation (rewards) earned as a function of time during the progressive ratio trial are shown for individual Cre+ mice. Mice earned between 7 and 11 pause rewards during the trial. All data plotted as means ±SEM.

Figure 7

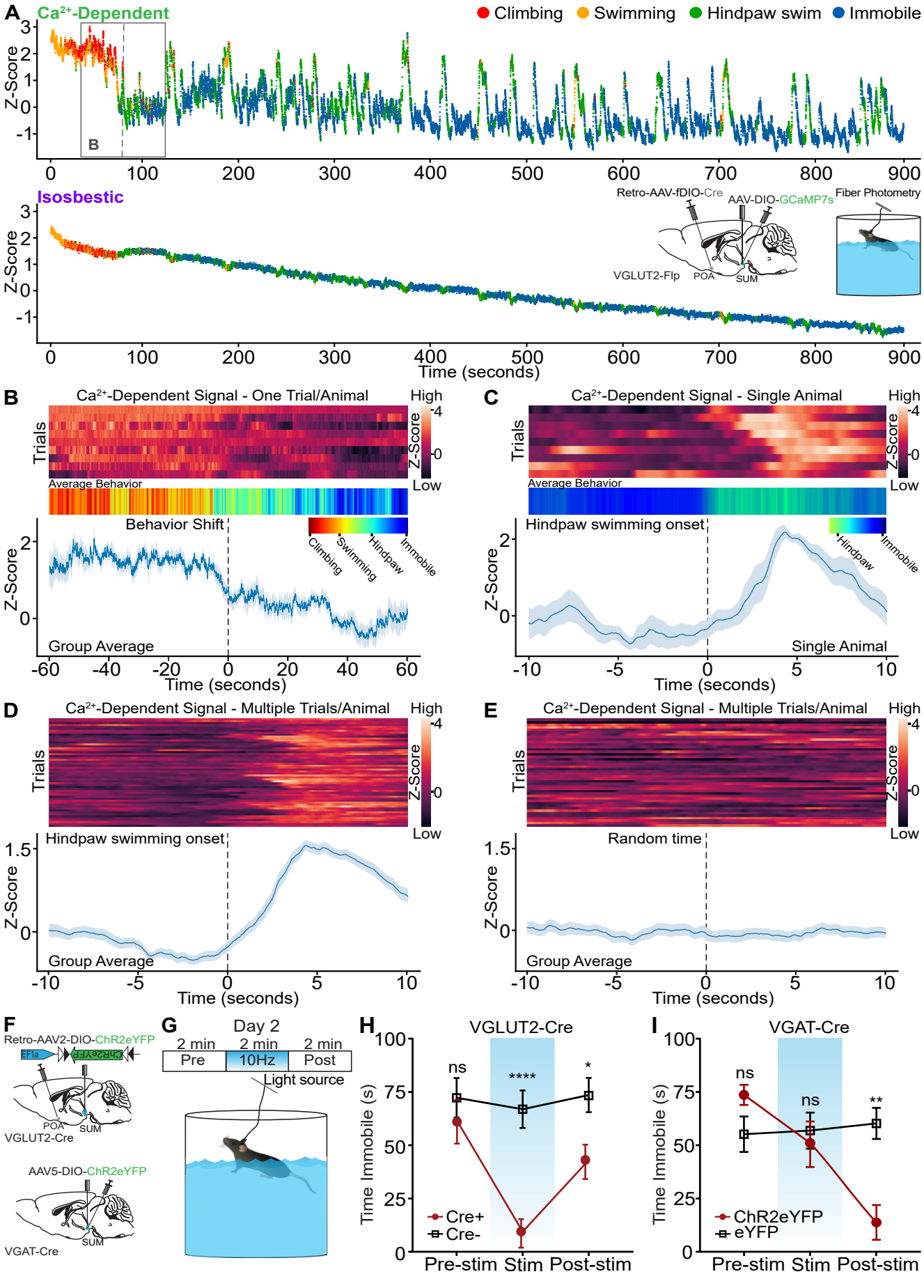
A
Ca2+-Dependent
Climbing
Swimming
Hindpaw swim
Immobile
Z-Score
B
Isosbestic
Retro-AAV-fDIO-Cre
AAV-DIO-GCaMP7s
Fiber Photometry
VGLUT2-Flp
POA
SUM
Time (seconds)
B
Ca2+-Dependent Signal - One Trial/Animal
Trials
High
Low
Average Behavior
Behavior Shift
Climbing
Swimming
Hindpaw
Immobile
Group Average
C
Ca2+-Dependent Signal - Single Animal
Hindpaw swimming onset
Single Animal
D
Ca2+-Dependent Signal - Multiple Trials/Animal
Hindpaw swimming onset
Group Average
E
Ca2+-Dependent Signal - Multiple Trials/Animal
Random time
Group Average
F
Retro-AAV2-DIO-ChR2eYFP
EF1a
ChR2eYFP
POA
SUM
VGLUT2-Cre
AAV5-DIO-ChR2eYFP
VGAT-Cre
G
Day 2
2 min
2 min
2 min
Pre
10Hz
Post
Light source
H
VGLUT2-Cre
Time Immobile (s)
ns
****
*
Cre+
Cre-
Pre-stim
Stim
Post-stim
I
VGAT-Cre
ns
ns
**
ChR2eYFP
eYFP

Figure 7. SuM$^{VGLUT2+}$::POA neurons are recruited during active coping, and activation is sufficient drive a switch to active coping. (**A**) Color-coded per video frame (dot color) behavior combined with normalized Ca^{2+} dependent and isosbestic fiber photometry signals. Scoring and analysis of climbing, swimming, hindpaw swimming, and immobility were completed using deep learning-based classification and quantification (LabGym) of recorded behavior. Inset shows injection, implants, and behavioral assay. Box highlights the time frame shown in B. (**B**) Heat maps for recordings obtained from mice (n=9) during forced swim, averaged color-coded behaviors, and mean ±SEM Z-score of Ca^{2+} dependent signal for 2-min period around behavioral shift from climbing and swimming to hindpaw swimming and immobility, showing significant (*95% CI) decline in the Ca^{2+} dependent signal. (**C**) Representative heat map, averaged behavior, and mean ±SEM Z-score of Ca^{2+} dependent signal for 20-second window around onset of hindpaw swim from a representative animal. (**D**) Representative heat map and mean ±SEM Z-score of Ca^{2+} dependent signal for 20-second window around onset of hindpaw swim from for events from nine mice. Engaging in hindpaw swim correlates with a brief, significant (***99.9% CI) increase in Ca^{2+} signal. (**E**) Representative heat map and mean ±SEM Z-score of Ca^{2+} dependent signal for 20-second window around random time points. (**F**) Schematic of injection and implant in VGLUT2-Cre or VGAT-Cre mice. (**G**) Illustration of testing paradigm on second forced swim test following 15-minute swim on first day. (**H**) The average time spent immobile during the pre-stimulation period was not significantly ($p>0.999$) different. During 10 Hz photostimulation VGLUT2-Cre+ mice engaged in vigorous swimming and the time spent immobile was significantly (****=$p<0.001$) less than Cre- mice. In the post-stimulation period, the time spent immobile remained significantly (*=0.047) lower in Cre+ mice compared to Cre-. (**I**) In VGAT-Cre+ mice expressing ChR2 (n=10), the average time spent immobile during the pre-stimulation period was not significantly ($p=0.218$) different compared to eYFP controls. Photostimulation did not significantly increase time immobile ($p>0.999$). However, there was a significant (**$p=0.001$) decrease in the time spent immobile compared to the post-stimulation period. For Ca^{2+} signal differences: *=95% CI, **=99% CI, ***=99.9% CI, ns=not significant.

Figure 8

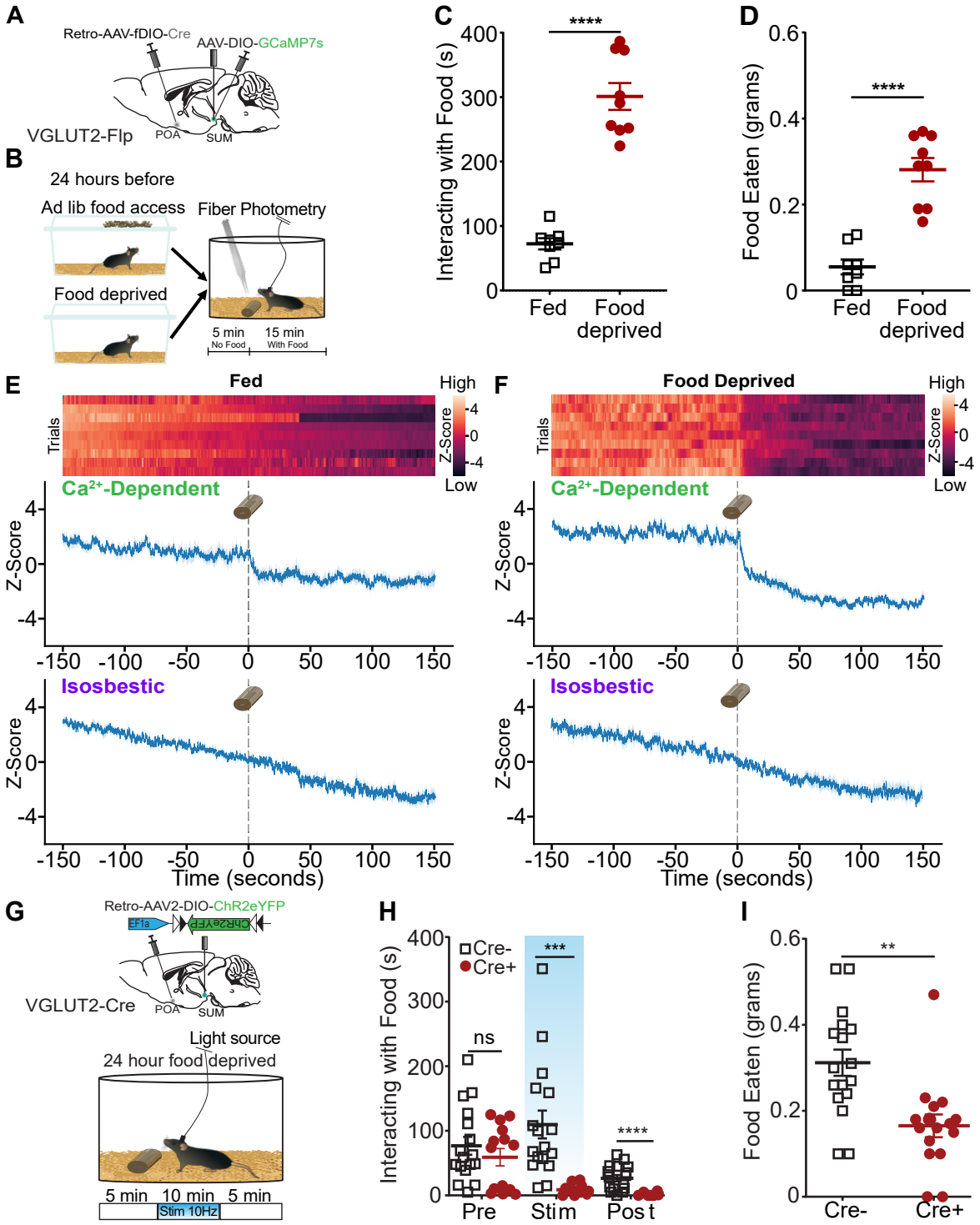
A
Retro-AAV-fDIO-Cre
AAV-DIO-GCaMP7s
VGLUT2-Flp
POA
SUM
B
24 hours before
Ad lib food access
Fiber Photometry
Food deprived
5 min
No Food
15 min
With Food
C
Interacting with Food (s)
****
Fed
Food deprived
D
Food Eaten (grams)
****
Fed
Food deprived
E
Fed
High
Low
Trials
Z-Score
Ca2+-Dependent
Isosbestic
Time (seconds)
F
Food Deprived
High
Low
Trials
Z-Score
Ca2+-Dependent
Isosbestic
Time (seconds)
G
Retro-AAV2-DIO-ChR2eYFP
EF1a
ChR2eYFP
VGLUT2-Cre
POA
SUM
Light source
24 hour food deprived
5 min
10 min
5 min
Stim 10Hz
H
Interacting with Food (s)
Cre-
Cre+
ns
***
****
Pre
Stim
Post
I
Food Eaten (grams)
**
Cre-
Cre+

Figure 8. Consummatory behavior suppresses SuM$^{VGLUT2+}$::POA neuron activity, and SuM$^{VGLUT2+}$::POA neuron blocks food consumption. (**A**) Schematic of injections in VGLUT2-Flp mice with AAV-DIO-GCaMP7s in SuM and Retro-AAV-fDIO-Cre in the POA and a fiber placed over SuM. (**B**) Mice were given ad lib food access or food deprived for 24 hours prior to testing. After being placed in the arena and allowed to habituate, mice were given a 20-minute trial divided into 5 mins of baseline and 15 mins after a chow pellet was added to the arena. (**C**) Food deprived mice (n=9) spent significantly ($p< 0.001$) more time interacting with the food pellet and (**D**) ate significantly ($p<0.001$) more than in the fed state. (**E**) Heat map and mean ±SEM Z-scores for Ca^{2+} dependent and isosbestic signals for recordings obtained from 9 animals show a small drop in (**E**) fed mice state (*95% CI) compared to a sharp decrease in Ca^{2+} activity after the introduction of the food pellet following addition in (**F**) food deprivation (***99.9% CI). (**G**) Mice were fasted for 24 hours prior to testing, and the schematized 20 min paradigm was used. Following food deprivation, animals were given access to a chow pellet. The trial was divided into 5-minute pre- and post-stimulation periods, with a 10-minute period of stimulation. (**H**) The time spent interacting with the food was quantified for each period. Cre+ (n=16) and Cre- (n=17) mice both rapidly engaged with the food pellet, and the average time spent interacting was not significantly ($p=0.37$) different. During the stimulation period and the post-stimulation period, the average time interacting with the food was significantly ($p=0.0002$, $p=0.0001$) lower in Cre+ mice compared to Cre- mice. (**I**) The food eaten during the total trial was calculated based on pellet weights, and, on average, Cre+ mice ate significantly ($p=0.001$) less food during the trial than Cre- mice. (**$p=0.001$, ***$p<0.001$, ****$p<0.0001$). For Ca^{2+} signal differences: *=95% CI, **=99% CI, ***=99.9% CI, ns=not significant.

Supplemental Figure 1

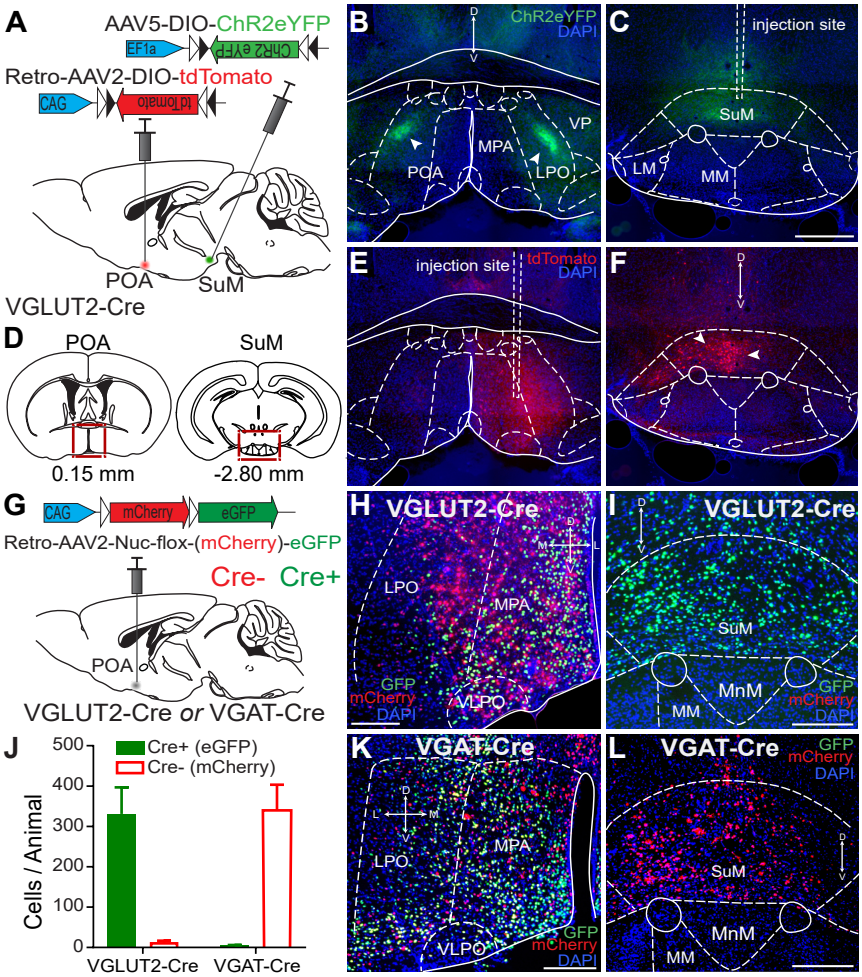

Supplemental Figure 1. SuM$^{VGLUT2+}$ neurons project to the preoptic area of the hypothalamus and are not VGAT+. (**A**) Schematic of injections into VGLUT2-Cre mice of Retro-AAV-DIO-tdTomato into the POA and AAV-DIO-ChR2eYFP into the SuM. (**B and C**) Projections of VGLUT2+ SuM neurons are evident in the POA with dense labeling in LPO and the site of viral injection in SuM (500um scale bar). (**D**) The brain regions, POA and SuM, shown in (B, C, E and F). (**E and F**) Cell bodies of VGLUT2+ SuM neurons are evident in SuM with injection of Retro-AAVs in POA. (**G**) Schematic of injection in POA of fluorophore switching construct in Retro-AAAV in VGLUT2-Cre or VGAT-Cre mice. (**H and I**) Labeling of Cre- (red) and Cre+ neurons in POA but only Cre+ seen in SuM of VLGUT2-Cre mice showing all SuM::POA neurons are VGLUT2+. (**J**) Quantification of labeling of Cre+ and Cre- cells in SuM following injections in POA in VGLUT2-Cre and VGAT-Cre mice. (**K and L**) Labeling of Cre- (red) and Cre+ neurons in POA but only Cre- seen in SuM of VGAT-Cre mice. (100um scale bar)

Supplemental Figure 2

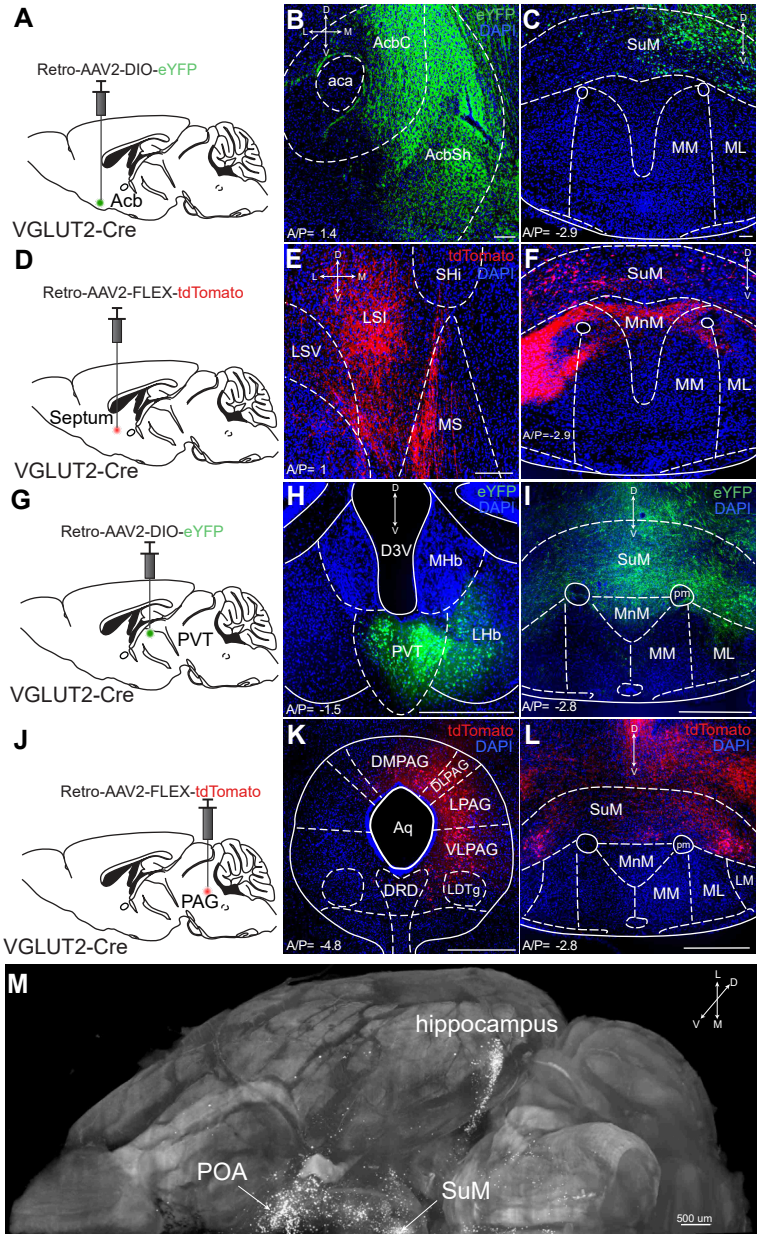

Supplemental Figure 2. Retrograde verification of projection targets of SuM$^{VGLUT2+}$::POA. (**A, D, G, and J**) Schematic showing the injection sites of Retro-AAV's in VGLUT2-Cre mice. (**B-C**) In VGLUT2-Cre mice, injection of Retro-AAV-DIO-eYFP unilaterally in the (**B**) accumbens nucleus resulted in labeling of cell bodies in (**C**) SuM. (E-F) Similarly, injection of Retro-AVV-DIO-tdTomato into (**E**) septum resulted in labeling of cell bodies in (**F**) SuM. (**H-I**) injection of Retro-AAV-DIO-eYFP targeting the (**H**) PV and lHb resulted in cell bodies in (**I**) SuM being labeled with eYFP. (**K-L**) Retro-AVV-DIO-tdTomato injected into (**K**) PAG labeled cells in (**L**) SuM. (**M**) The cleared brain hemisphere from a VGLUT2-Flp mouse injected in the POA with injected Retro-AAV-DIO-eYFP shown in Figure 2M displayed from a perspective of ventral to dorsal shows cells labeled in SuM and processes extending widely, including in the hippocampus and POA. (100 and 500 µm scale bars)

Supplemental Figure 3

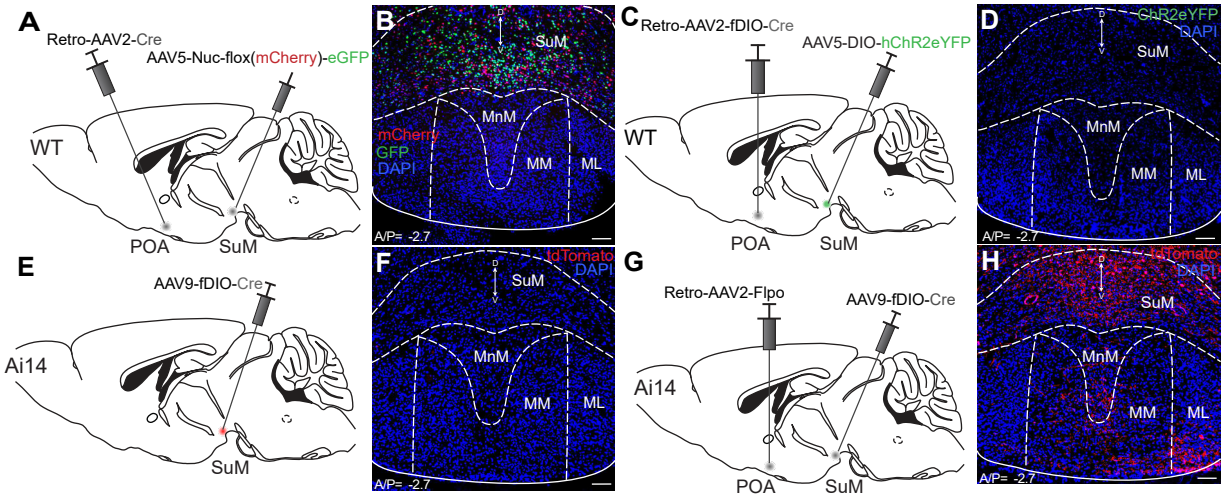

Supplemental Figure 3. Combinatorial viral and genetic approach is effective with minimal background. (**A**) Schematic of injection of Retro-AAV-Cre into the POA and AAV-Nuc-flox(mCherry)-eGFP into the SuM of WT mice. (**B**) In SuM, eGFP (green) Cre+ and mCherry (red) Cre- labeled neurons are seen based on expression of Cre mediated by POA injected retrograde AAV constructs showing SuM::POA neurons are a subset of all cells in SuM. (**C and D**) In wildtype mice injected in POA with Retro-AAV-fDIO-Cre and in SuM with AAV-DIO-ChR2eYFP, expression of ChR2eYFP (green) is not seen. (**E-H**) In Ai14 reporter mice injected with AAV-fDIO-Cre into SuM, tdTomato expression is not observed unless Retro-AAV2-Flp is injected. (100 µm scale bars)

Supplemental Figure 4

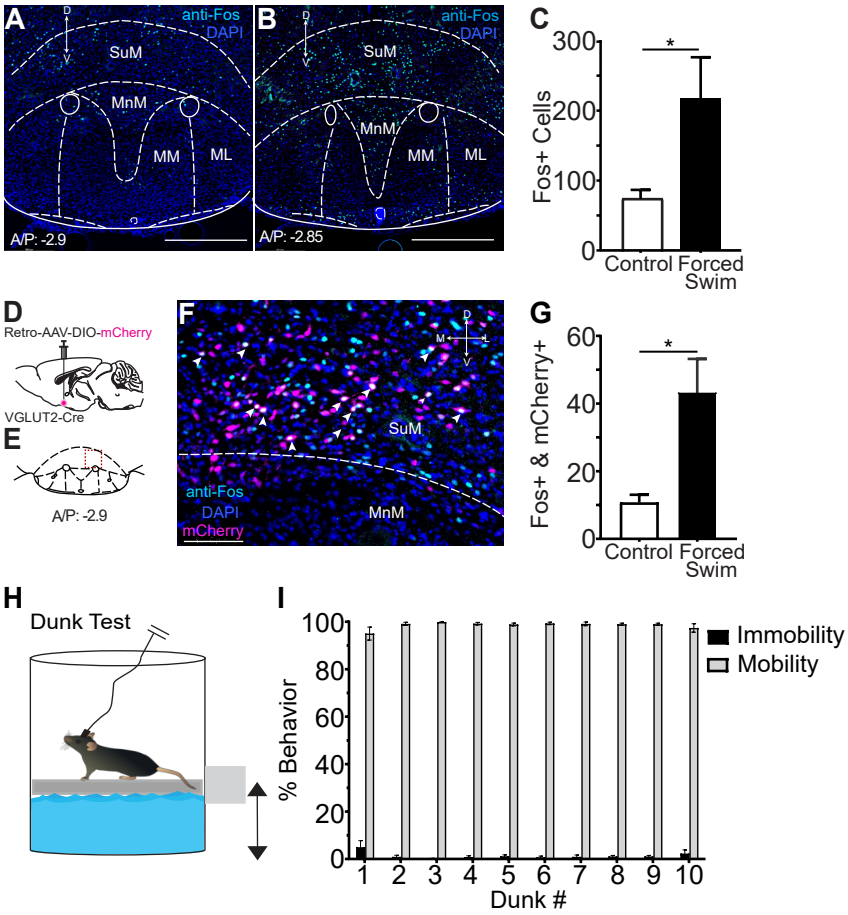

Supplemental Figure 4. SuM$^{VGLUT2+}$::POA neurons show Fos induction after FST, and dunk test evokes active coping. Sections of brains from mice (**A**) left in the home cage or (**B**) subjected to 15 minutes of forced swimming 90 min prior to sacrifice were probed with anti-Fos antibodies (cyan) showed (scale bars 500μm) (**C**) a significant (p= 0.029) increase in the mean ±SEM number of anti-Fos labeled neurons in brains from mice subjected to force swim (n=5) compared to control mice (n=4). (**D**) In VLGUT2-Cre mice, Retro-AAV-DIO-mCherry was injected in the POA of mice (n=5) subjected to 15 minutes forced swim. (**E**) Region of SuM shown with higher magnification in (**F**) where SuM$^{VGLUT2+}$::POA neurons labeled by mCherry show overlap with cells (arrows) labeled by anti-Fos. (Scale bar 100μm) (**G**) A significant increase (p= 0.016) in the number of VGLUT2+ cells labeled with mCherry and anti-Fos is seen in mice subjected to forced swim. (**H**) Mice subjected to 10 30-second trials of “dunk” forced swimming. (**I**) Quantitation of average time mobile for every 30-second trial during “dunk” forced swim.

Supplemental Figure 5

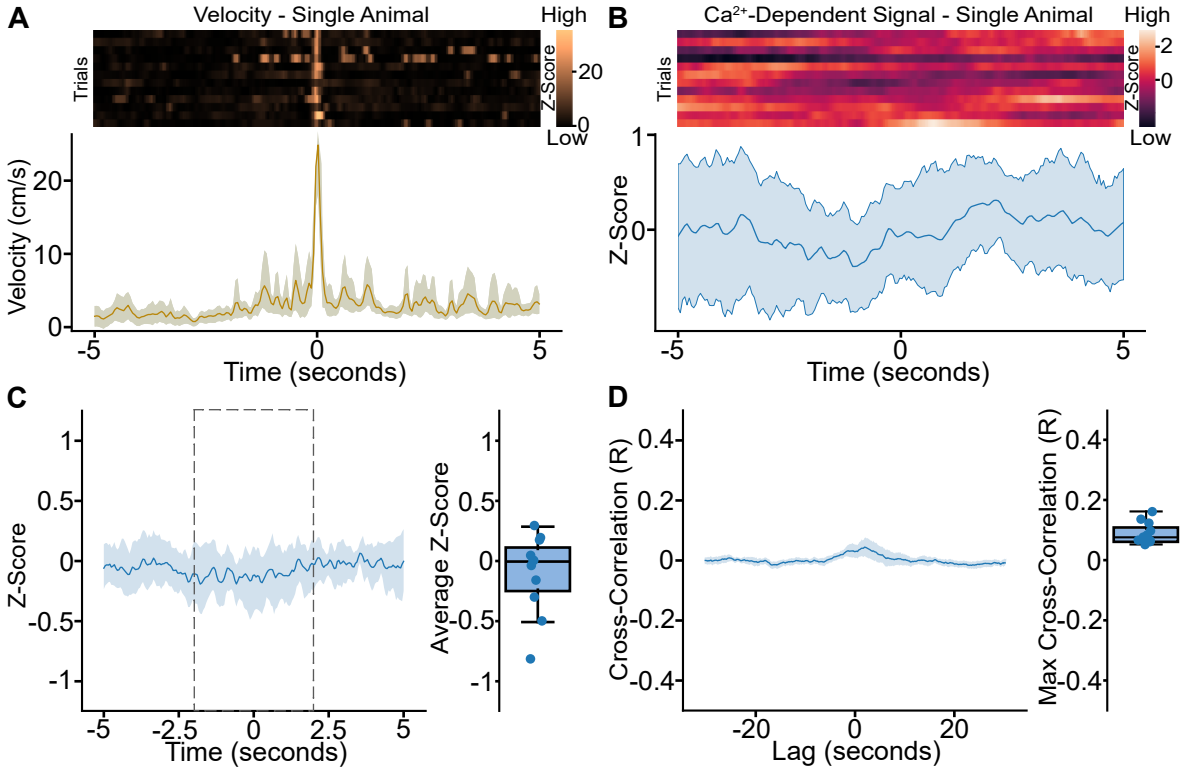

Supplemental Figure 5. SuM$^{VGLUT2+}$::POA neurons are not recruited during increased locomotor activity in the absence of acute stressor. (**A**) Heat maps showing velocity for 12 episodes of rapid locomotion from a representative animal during free movement in open field with mean ±95% CI for the trials. (**B**) For that same animal, heat maps of Ca^{2+}-dependent signal were analyzed during average peak velocity, showing no change in activity during peak velocity. Representative heat map for a single animal with the mean ±95% confidence interval of the 12 trials for same animal. (**C**) Mean ±95% confidence interval for Z-score of 12 trials for all 13 animals and Boxplot for average Z-score. (**D**) Cross-correlation analysis shows no correlation between Ca^{2+} signal from SuM$^{VGLUT2+}$::POA neurons and spontaneous velocity increases.

Supplemental Figure 6

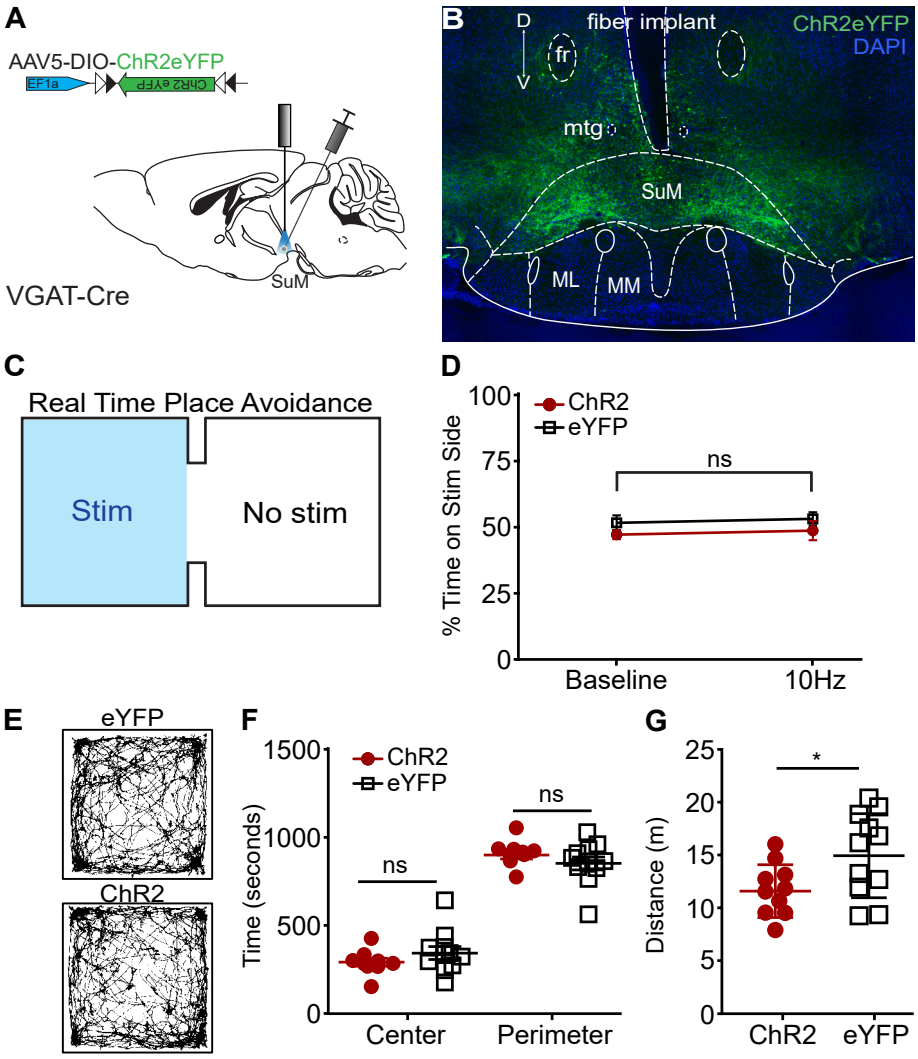

Supplemental Figure 6. GABAergic neurons in SuM do not drive place preference. (**A**) Schematic of viral injection into VGAT-Cre mice in SuM. (**B**) VGAT+ neurons labeled and outline of implanted fiber. (**C**) Real-time arena showing the pair of photostimulation on one side of the arena. (**D**) Photostimulation at 10 Hz did not drive a significant place preference (p = 0.67). (eYFP (control) n=26 and ChR2=26). All data plotted as mean ±SEM. (**E**) Representative path traces of VGAT-Cre mice with ChR2 or eYFP (control) in open field testing. (**F**) No significant differences in center (p=0.254) or perimeter (p=0.287) time when comparing the ChR2eYFP expressing to controls VGAT-Cre mice. (**G**) Chr2eYFP expressing mice traveled slightly but significantly (p=0.034) less distance compered to control.

Supplemental Figure 7

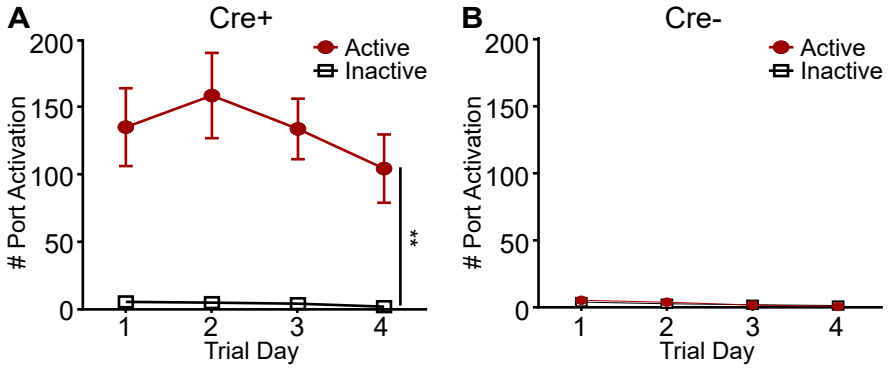

Supplemental Figure 7. SuMVGLUT2+::POA stimulations drives active port activation. (A) Cre+ mice activated the active port significantly more (**p=0.001) compared to the inactive port. **(B)** In Cre- mice, no significant change in the number of port activations of both the active and inactive ports.

Supplemental Table 1

Figure	Panel	Test	Statistic	P value	Bonferroni's Multiple comparisons	Multiple comparisons statistic	Adjusted P value
3	G	T-Confidence Interval	95% CI -30 to 0s [-0.73511383 -0.724353688] 1 to 30s [1.903893784 1.965866945] Difference [2.630811087 2.694498841] 99% CI -30 to 0s [-0.737419984 -0.718129215] 1 to 30s [1.894157095 1.975603635] Difference [2.620805016 2.704550491] 99.9% CI -30 to 0s [-0.74009622 -0.715452978] 1 to 30s [1.882857892 1.986902837] Difference [2.609193202 2.716116722]	Sig at 95% Sig at 99% Sig at 99.9%	N/A	N/A	N/A
	I	T-Confidence Interval	95% CI -3 to -1s [0.213736241 0.298523885] 1 to 3s [5.190328104 6.484427377] Difference [4.932810735 6.22968462] 99% CI -3 to -1s [0.200415137 0.311844989] 1 to 3s [4.987010372 6.687745109] Difference [4.72905708 6.433438275] 99.9% CI -3 to -1s [0.184956303 0.327303822] 1 to 3s [4.751064858 6.923690623] Difference [4.492605688 6.669889668]	Sig at 95% Sig at 99% Sig at 99.9%	N/A	N/A	N/A
	J	T-Confidence Interval	95% CI -3 to -1s [1.116192035 1.439691613] 1 to 3s [0.049420441 0.369842849] Difference [-1.295973579 -0.840646778] 99% CI -3 to -1s [1.065366568 1.49051708] 1 to 3s [-0.000921568 0.420184858] Difference [-1.367510605 -0.769109753] 99.9% CI -3 to -1s [1.006384792 1.549498856] 1 to 3s [-0.059342302 0.478605592] Difference [-1.450527664 -0.686092694]	Sig at 95% Sig at 99% Sig at 99.9%	N/A	N/A	N/A

Supplemental Table 1 cont.

	K	T-Confidence Interval	95% CI -3 to -1s [-0.21380383 0.000116753] 1 to 3s [-0.381118104 -0.039309855] Difference [-0.304985727 0.098244846] 99% CI -3 to -1s [-0.24741319 0.033726113] 1 to 3s [-0.434820072 0.014392113] Difference [-0.368337842 0.16159696] 99.9% CI -3 to -1s [-0.286416073 0.072728995] 1 to 3s [-0.497139961 0.076712002] Difference [-0.441856502 0.235115621]	ns ns ns	N/A	N/A	N/A
4	C	Two-Way RM ANOVA	Stimulation Period x Genotype F (2, 58) = 12.82 Stimulation Period F (1.012, 29.36) = 12.27 Genotype F (1, 29) = 11.78	p<0.001**** p=0.0014** p=0.0018**	Pre-stimulation Stimulation Post-stimulation	t=1 t=3.429 t=1	p=0.9995 p=0.0122* p=0.9995
	D	Two-Way RM ANOVA	Stimulation Period x Genotype F (2, 58) = 21.04 Stimulation Period F (1.794, 52.02) = 18.34 Genotype F (1, 29) = 0.6615	p<0.001**** p<0.001**** p=0.4227	Pre-stimulation Stimulation Post-stimulation	t=1.02 t=3.74 t=3.281	p=0.9495 p=0.0039** p=0.0139*
	E	Two-Way RM ANOVA	Stimulation Period x Genotype F (2, 58) = 14.84 Stimulation Period F (1.667, 48.34) = 6.658 Genotype F (1, 29) = 4.707	p<0.0001**** p=0.0045** p=0.0384*	Pre-stimulation Stimulation Post-stimulation	t=0.7131 t=3.267 t=3.81	p>0.9999 p=0.0156* p=0.0052**
5	C	Two-Way ANOVA	Frequency x Genotype F (4, 188) = 36.76 Frequency F (4, 188) = 34.61 Genotype F (1, 188) = 352.1	p<0.0001**** p<0.0001**** p<0.0001****	Cre+ vs Cre- 1 Hz 5 Hz 10 Hz 20 Hz	 t=4.477 t=10.09 t=12.36 t=15.09	 p<0.0001**** p<0.0001**** p<0.0001**** p<0.0001****
	D	Two-Way Mixed Model ANOVA	Time x Genotype F (9.116, 218.1) = 1.418 Time F (1, 24) = 0.02824 Genotype F (29, 694) = 1.038	p=0.1807 p=0.868 p=0.4125	N/A	N/A	N/A
	E	Two-Way Mixed Model ANOVA	Time x Genotype F (29, 694) = 1.035 Time F (7.228, 173.0) = 1.030 Genotype F (1, 25) = 90.74	p=0.4159 p=0.4124 p<0.0001****	N/A	N/A	N/A
	F	Two-Way ANOVA	Frequency x Genotype F (4, 115) = 12.37 Frequency F (4, 115) = 12.38 Genotype F (1, 115) = 187.5	p<0.0001**** p<0.0001**** p<0.0001****	Cre+ vs Cre- 1 Hz 5 Hz 10 Hz 20 Hz	 t=4.117 t=7.622 t=8.789 t=9.156	 p=0.0004*** p<0.0001**** p<0.0001**** p<0.0001****
	H	Two-Tailed T-Test Two-Tailed T-Test	Center Cre+ vs Cre- t=1.407, df=36 Perimeter t=1.356, df=36	 p=0.1681 p=0.1837	N/A	N/A	N/A
	I	Two-Tailed T-Test	Total Distance t=4.857, df=33	 p<0.0001****	N/A	N/A	N/A

Supplemental Table 1 cont.

	K	Two-Tailed T-Test	Time in dark eYFP vs ChR2 t=0.4208, df=15	p=0.6799	N/A	N/A	N/A
	L	Two-Tailed T-Test	Distance eYFP vs ChR2 t=3.516, df=15	p=0.0031**	N/A	N/A	N/A
6	C	Two-Way RM ANOVA	Day x Genotype F (3, 60) = 18.15 Day F (1.945, 38.89) = 8.547 Genotype F (1, 20) = 255.7	p<0.0001**** p=0.0009*** p<0.0001****	Cre+ vs Cre- Day1 Day 2 Day 3 Day 4	 t=6.368 t=14.31 t=20.64 t=10.93	 p=0.0003*** p<0.0001**** p<0.0001**** p<0.0001****
	D	Two-Way RM ANOVA	Day x Genotype F (3, 60) = 0.9819 Day F (2.047, 40.94) = 1.251 Genotype F (1, 20) = 41.10	p=0.4074 p=0.2975 p<0.0001****	Cre+ vs Cre- Day1 Day 2 Day 3 Day 4	 t=4.756 t=5.669 t=4.839 t=3.798	 P<0.0001**** p<0.0001**** p<0.0001**** p<0.0011**
	E	Mixed-Model RM ANOVA	Day x Genotype F (3, 72) = 3.449 Day F (1.871, 44.91) = 0.6416 Genotype F (1, 72) = 51.92	p=0.021* p=0.5212 p<0.0001****	Cre+ vs Cre- Day1 Day 2 Day 3 Day 4 Cre+ Day Comparisons Day1 vs. Day 2 Day1 vs. Day 3 Day1 vs. Day 4	 t=2.133 t=3.246 t=4.432 t=2.903 t=3.099 t=3.387 t=3.241	 p=0.0455* p=0.0087** p=0.003** p=0.0336* p=0.0338* p=0.0208* p=0.0265*
	F	Two-Tailed T-Test Two-Tailed T-Test Two-Tailed T-Test	Active nose poke t=12.54, df=20 Inactive nose poke t=3.709, df=20 Rewards t=18.78, df=20	p<0.001**** p=0.0014** p<0.001****	N/A	N/A	N/A
7	B	T-Confidence Interval	95% CI -60 to 0s [0.959541188 1.952620738] 0 to 60s [-0.355286068 0.726943754] Difference [-2.004661471 -0.535842769] 99% CI -60 to 0s [0.803517083 2.108644843] 0 to 60s [-0.525316696 -0.896974382] Difference [-2.235429614 -0.305074626] 99.9% CI -60 to 0s [0.622454726 2.2897072] 0 to 60s [-0.722633299 1.094290984] Difference [-2.503230695 -0.037273545]	Sig at 95% ns ns	N/A	N/A	N/A
	D	T-Confidence Interval	95% CI -10 to 0s [-0.506739492 -0.126437473] 0 to 10s [0.197230326 0.726601455] Difference [0.452596634 1.104412112] 99% CI -10 to 0s [-0.566489269 -0.066687695] 0 to 10s [0.114060094 0.809771688] Difference [0.350189 1.206819746]	Sig at 95% Sig at 99%	N/A	N/A	N/A

Supplemental Table 1 cont.

			99.9% CI -10 to 0s [-0.635827501 0.002650537] 0 to 10s [0.017542967 0.906288814] Difference [0.231347315 1.325661431]	Sig at 99.9%			
	E	T-Confidence Interval	95% CI -10 to 0s [-0.265038212 0.2702523] 0 to 10s [-0.237081362 0.254877431] Difference [-0.357219458 0.36980144] 99% CI -10 to 0s [-0.349138447 0.354352535] 0 to 10s [-0.31437369 0.332169759 Difference [-0.47144272 0.484024702] 99.9% CI -10 to 0s [-0.44673482 0.451948908] 0 to 10s [-0.404069645 0.421865715] Difference [-0.603996167 0.616578149]	ns ns ns	N/A	N/A	N/A
	H	Two-Way RM ANOVA	Stimulation Period x Genotype F (2, 36) = 8.208 Stimulation Period F (1.701, 30.62) = 12.93 Genotype F (1, 18) = 10.11	 0.0012** 0.0002*** 0.0052**	 Pre-stimulation Stimulation Post-stimulation	 t=0.7599 t=5.2 t=2.677	 p>0.9999 p=0.0002**** p=0.0465*
	I	Two-Way RM ANOVA	Stimulation Period x Genotype F (2, 40) = 14.09 Stimulation Period F (1.995, 39.90) = 10.01 Genotype F (1, 20) = 1.898	 p<0.0001**** p=0.0003*** p=0.1835	 Pre-stimulation Stimulation Post-stimulation	 t=1.923 t=0.7005 t=4.238	 p=0.2183 p>0.9999 p=0.0012**
8	C	Two-Tailed T-Test	Fed vs Fasted t=9.666, df=15	 p<0.0001****	N/A	N/A	N/A
	D	Two-Tailed T-Test	Fed vs Fasted t=6.807, df=15	 p<0.0001****	N/A	N/A	N/A
	E	T-Confidence Interval	Isosbestic 95% CI -150 to -10s [-0.127314348 0.690501429] 10 to 150s [0.709907655 1.43150582] Difference [0.243786104 1.334440291] 99% CI -150 to -10s [-0.255802519 0.818989599] 10 to 150s [0.596536367 1.544877109] Difference [0.072431912 1.505794483] 99.9% CI -150 to -10s [-0.404910063 0.968097143] 10 to 150s [0.464971614 1.676441861] Difference [-0.126420656 1.704647051] Ca^{2+} -Dependent 95% CI -150 to -10s [0.024359471 0.477339678]	 Sig at 95% ns ns Sig at 95%	N/A	N/A	N/A

Supplemental Table 1 cont.

			10 to 150s [0.564052895 1.293569678] Difference [0.248605856 1.107317568] 99% CI -150 to -10s [-0.046808878 0.548508026] 10 to 150s [0.449437502 1.408185071] Difference [0.113692468 1.242230956] 99.9% CI -150 to -10s [-0.129398096 0.631097245] 10 to 150s [0.316428994 1.541193579] Difference [-0.042871391 1.398794816]	 ns ns			
	F	T-Confidence Interval	Isosbestic 95% CI -150 to -10s [0.049394291 0.689096421] 10 to 150s [0.670463682 1.423655887] Difference [0.183719975 1.171908881] 99% CI -150 to -10s [-0.051110197 0.78960091] 10 to 150s [0.55212861 1.541990959] Difference [0.028464246 1.32716461] 99.9% CI -150 to -10s [-0.167743327 0.906234039] 10 to 150s [0.414803502 1.679316067] Difference [-0.151706429 1.507335286] Ca^{2+} -Dependent 95% CI -150 to -10s [-0.875926952 0.142125648] 10 to 150s [1.203199181 1.724507405] Difference [1.258872541 2.402635349] 99% CI -150 to -10s [-1.035874608 0.302073304] 10 to 150s [1.121295723 1.806410863] Difference [1.07917438 2.582333509] 99.9% CI -150 to -10s [-1.221490155 0.487688851] 10 to 150s [1.026248658 1.901457927] Difference [0.87063883 2.79086906]	 ns ns ns Sig at 95% Sig at 99% Sig at 99.9%	N/A	N/A	N/A
	H	Two-Way RM ANOVA	Stimulation Period x Genotype F (2, 58) = 8.330 Stimulation Period F (1.884, 54.64) = 13.21 Genotype F (1, 29) = 14.81	 p=0.0007*** p<0.0001**** p=0.0006***	Cre+ vs Cre- Pre-stimulation Stimulation Post-stimulation Cre+	 t=0.9168 t=4.68 t=5.192	 p>0.9999 p=0.0007*** p=0.0002***

Supplemental Table 1 cont.

					Pre stim vs. Stim Pre stim vs. Post stim Stim vs. Post stim	t=3.725 t=4.285 t=3.662	p=0.0153* p=0.0053** p=0.0172*
	I	Two-Tailed T-Test	Cre+ vs Cre- t=3.621, df=31	p=0.001**	N/A	N/A	N/A
Supp Fig 4	C	Mann-Whitney	Control vs FST	p=0.0286*	N/A	N/A	N/A
	G	Mann-Whitney	Control vs FST	p=0.0159*	N/A	N/A	N/A
Supp Fig 6	D	Two-Way RM ANOVA	Stimulation Period x Genotype F (1, 29) = 0.002860 Stimulation Period F (1, 29) = 0.04236 Genotype F (1, 29) = 1.790	p=0.9577 p=0.8384 p=0.1914	Cre+ Baseline vs 10Hz Cre+ vs Cre- Baseline 10 Hz	t=0.1864 t=0.8956 t=0.9722	p>0.9999 p=0.7483 p=0.67
	F	Two-Tailed T-Test Two-Tailed T-Test	Center t=1.175, df=19 Perimeter t=1.094, df=19	p=0.254425 p=0.287443	N/A	N/A	N/A
	G	Two-Tailed T-Test	Distance t=2.278, df=19	p=0.0345*	N/A	N/A	N/A
Supp Fig 7	A	Two-Way RM ANOVA	Day x Activity State F (3, 60) = 0.99 Day F (2.0, 41) = 1.2 Activity state F (1, 20) = 40	p=0.41 p=0.3 p=0.001**	N/A	N/A	N/A
	B	One-Way RM ANOVA	Day F (2.537, 25.37) = 3.042	p=0.0546	N/A	N/A	N/A

Supplemental Table1. Statistical analyses and values.